Magnetic field structure in star-forming regions

C. Eswaraiah, W. P. Chen
Institute of Astronomy
National Central University
Taiwan

Collaborators
M. Tamura, NAOJ, Japan
Shih-Ping Lai, NTHU, Taiwan
D. P. Clemens, BU, Boston, USA
A. K. Pandey, ARIES, India
D. K. Ojha, TIFR, India

Magnetic fields at different scales:

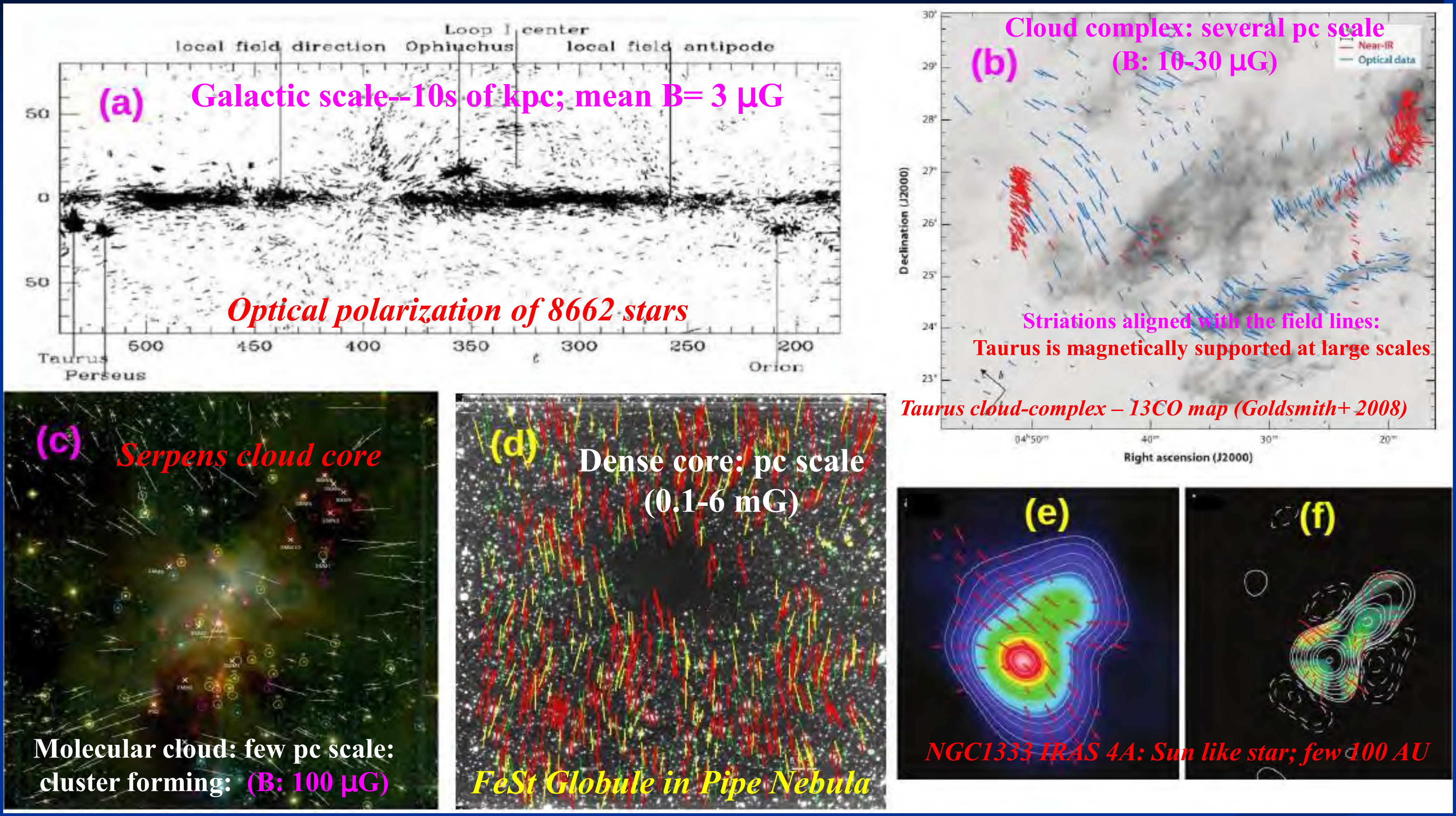

(a) Heiles & Crutcher (2005) (b) Chapman+ 2011 (c) Sugitani+ 2010, (d) Clemens+ (In preparation): NIR H-band polarimetry of FeSt Globule in Pipe Nebula (e) Girart+ (2006; SMA 0.87 mm) (f) S. P. Lai (Private communication)

After the onset of star-formation – feedback process, mid-infrared bubbles – filaments vs magnetic fields

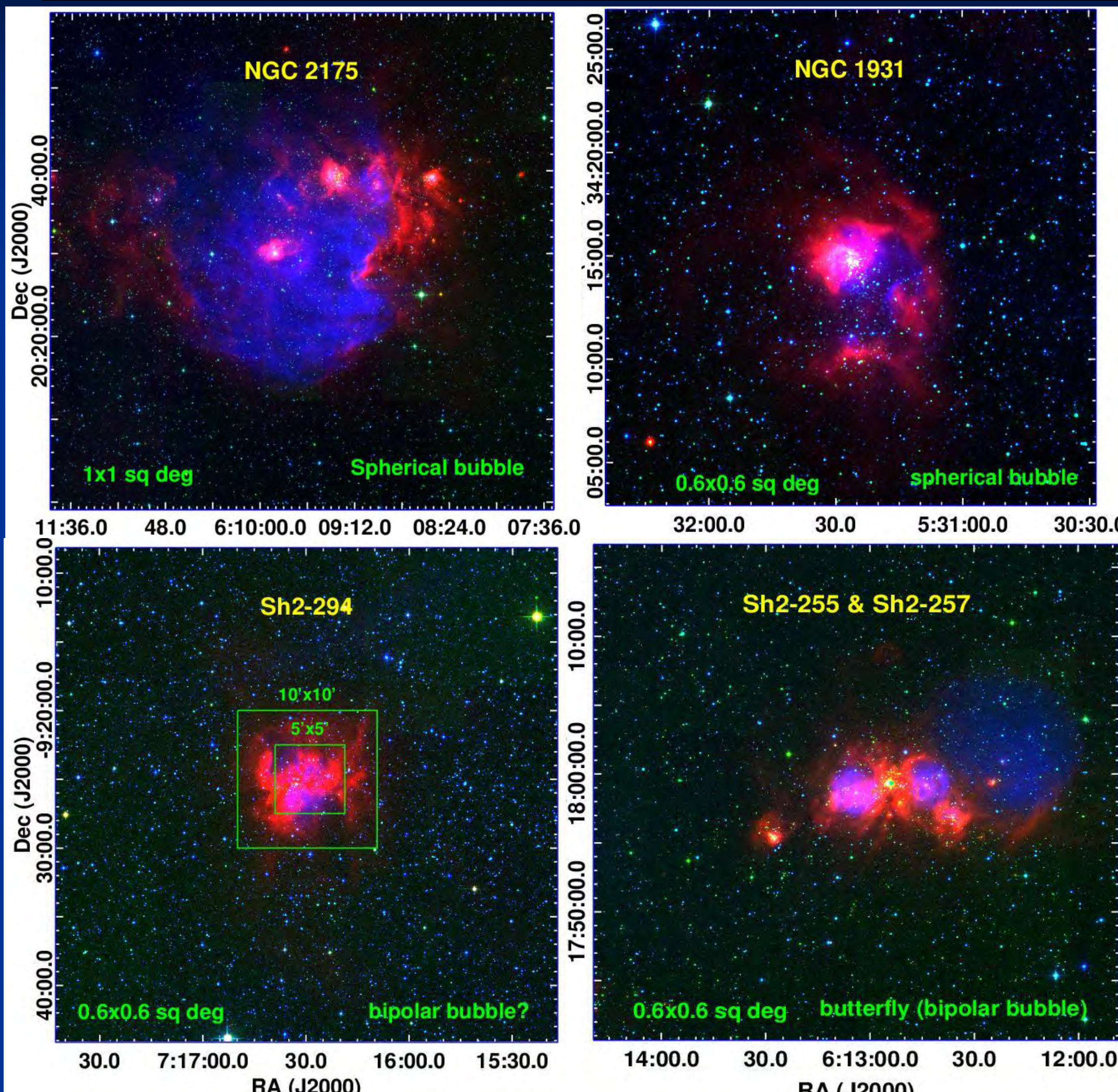

- Massive stars (O/B) – stellar winds, and UV-radiation
- Inhomogeneous ISM – expansion of I-front and shock front can create – spherical/arc shaped shells, Bright Rimmed Clouds (pillars, elephant trunks, cometary globules)
- Induce - second generation star-formation

* Triggered star-formation

To study:

- How the bipolar (butterfly / hourglass shaped) bubbles created?
- Any link between the filaments and bipolar bubbles?
- Magnetic field vs filament, bubble formation (feed back)?
- Also the influence of B-fields on formation and evolution of BRCs?

Targets

- RCW57A – bipolar bubble, NIR-polarimetry with SIRPOL
- NGC 1893 – active star-forming region – 2 elephant trunks (Sim129, Sim130) – optical (AIMPOL), NIR (SIRPOL + Mimir instrument) polarimetry
- LDN1225 – dark globule towards Cep OB3 cloud complex– large scale filament -fragmented – optical (AIMPOL) and NIR (Planned with Mimir instrument)

Principle: differential extinction by aligned dust grains - dichroism

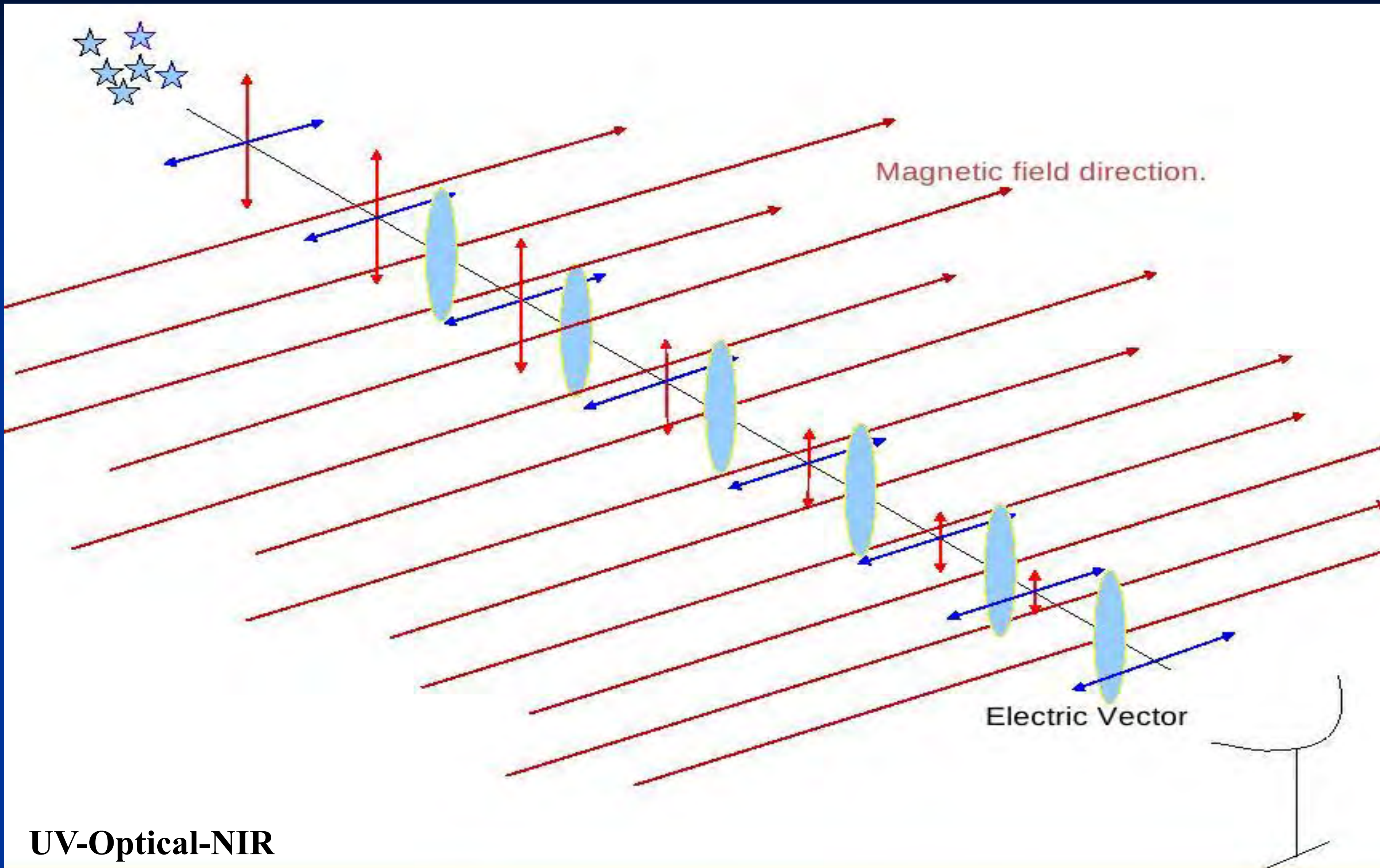

Polarization direction: **line-of-sight-averaged plane-of-the-sky-magnetic field direction.**
The detailed process(es) - aligned dust grains wrt magnetic fields has (have) long been, and is still actively, under study (Davis & Greenstein 1951; Dolginov 1990; Lazarian 2003, Cho & Lazarian 2005).

Polarization, Stokes parameters: I, Q, U and V

Total incoming light can be represented
as a combination of following stokes parameters:

$$I^2 = Q^2 + U^2 + V^2$$

I: **Total intensity**
Q, U: **linear polarization**
V: **circularly polarization**

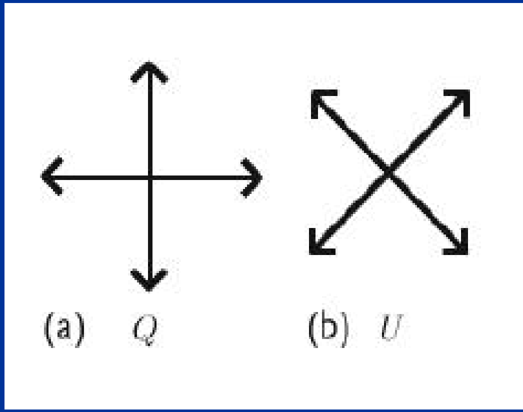

q=Q/I, u=U/I

Polarization (%) **P = sqrt(q^2 +u^2)**

And

Polarization Angle (radians) **PA= 0.5 arctan(u/q)**

Instrument: AIMPOL (optical)

1.04m Sampurnanad Telescope, ARIES, INDIA

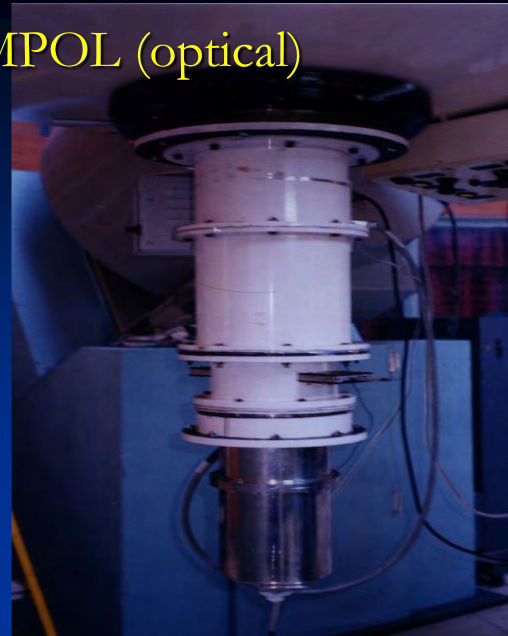

AIMPOL (ARIES Imaging POLarimeter)

ARIES IMaging Polarimeter (AIMPOL)

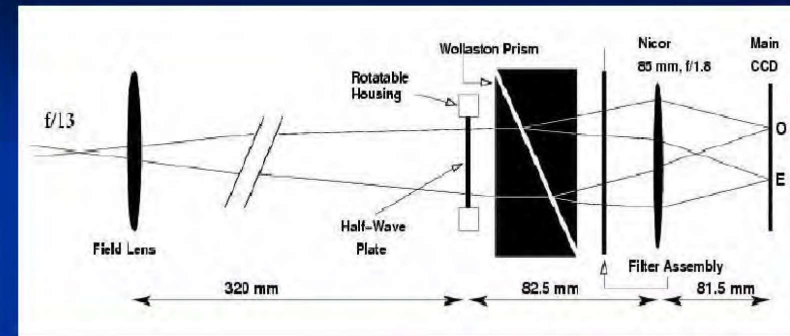

HALF WAVE PLATE BEAM SPLITTER FOCAL REDUCER

Optical Layout of AIMPOL (Rautela et al. 2004)

SIRPOL: SIRIUS (Simultaneous IR Imager for Unbiased Survey) polarimetry mode On IRSF (IR Survey Facility) 1.4 m telescope at Sutherland, South Africa

A schematic view of IRSF/SIRPOL

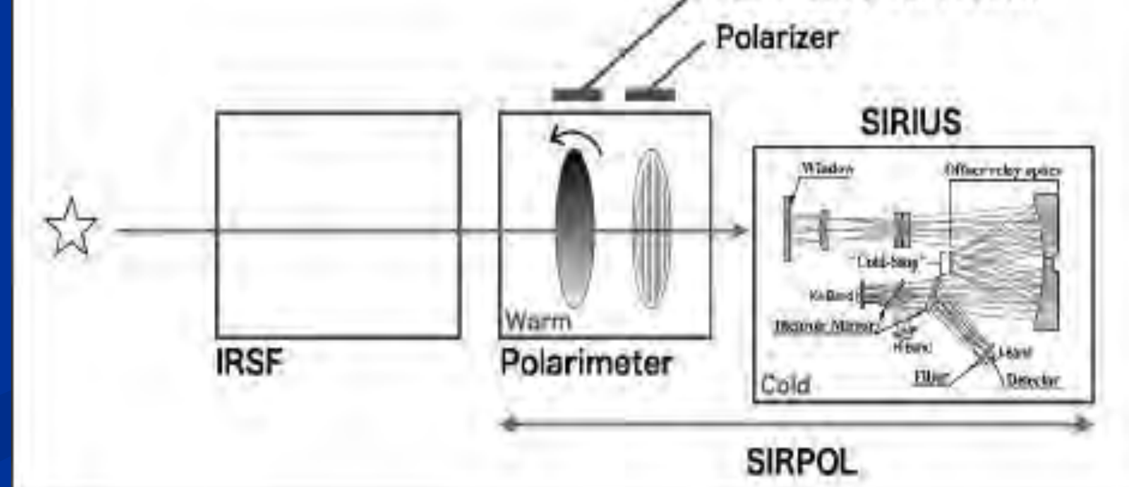

RCW57A

• A star forming cloud region: NGC 3576/RCW 57A: distance of ~2.4-2.8 kpc, eight O7.5V stars, five IRS sources, six H2O masers, yet unrecognised O type stars - would account of Lyα photons, star formation is still actively ongoing, (Eswaraiah, Chen+ to be submitted)

Wise 4.6 micron (Red), 2 MASS K-band (green), DSS-II R-band (blue)

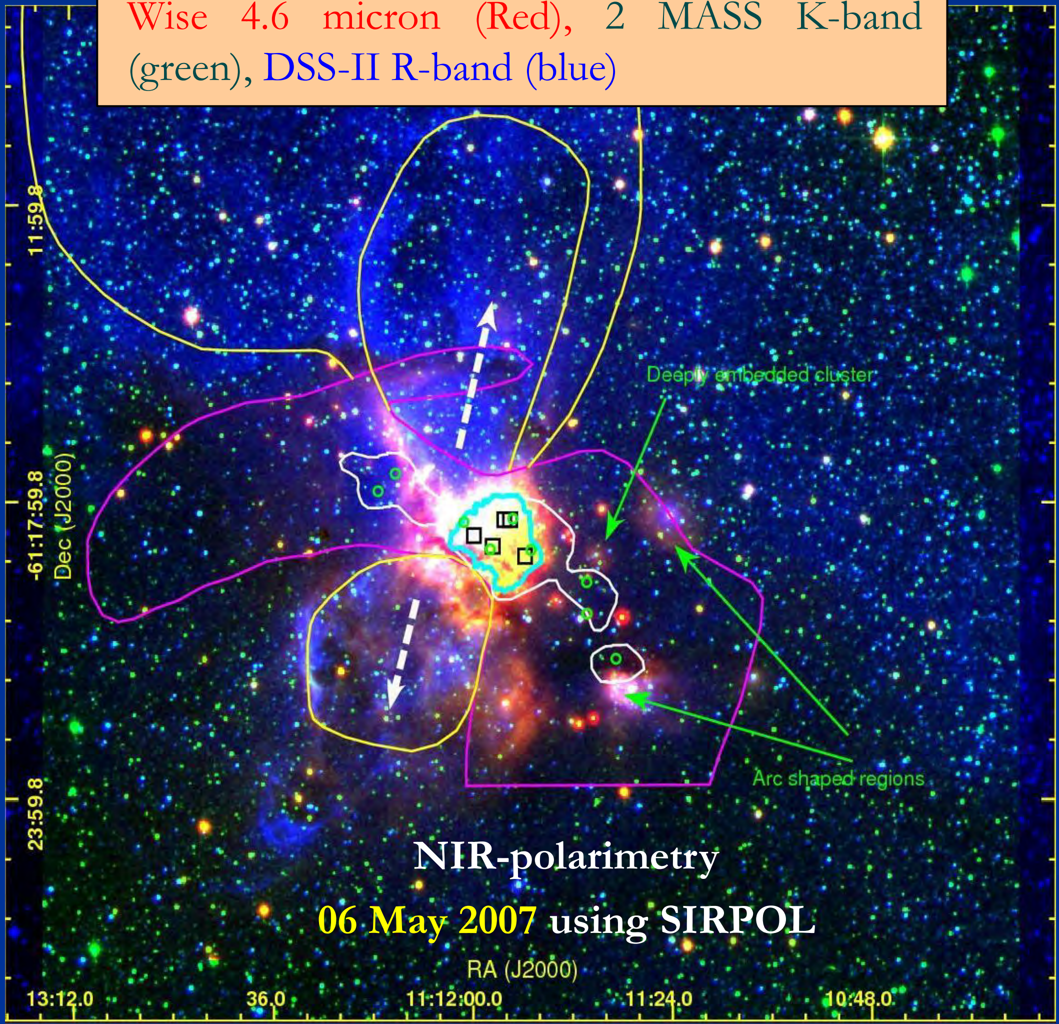

NIR-polarimetry

06 May 2007 using SIRPOL

Yellow: extent of bubble based on Halpha, Spitzer, WISE images.

Cyan: 3.4 cm radio emission.

White: 1.2 mm dust continuum emission.

Magenta: extent of molecular cloud - 13CO map

Black squares: IRS sources.

Green circles: water masers

White arrows: possible out-flow direction.

(Purcell+ 2009, and references therein)

Distribution of NIR colours:
RCW57A versus control field

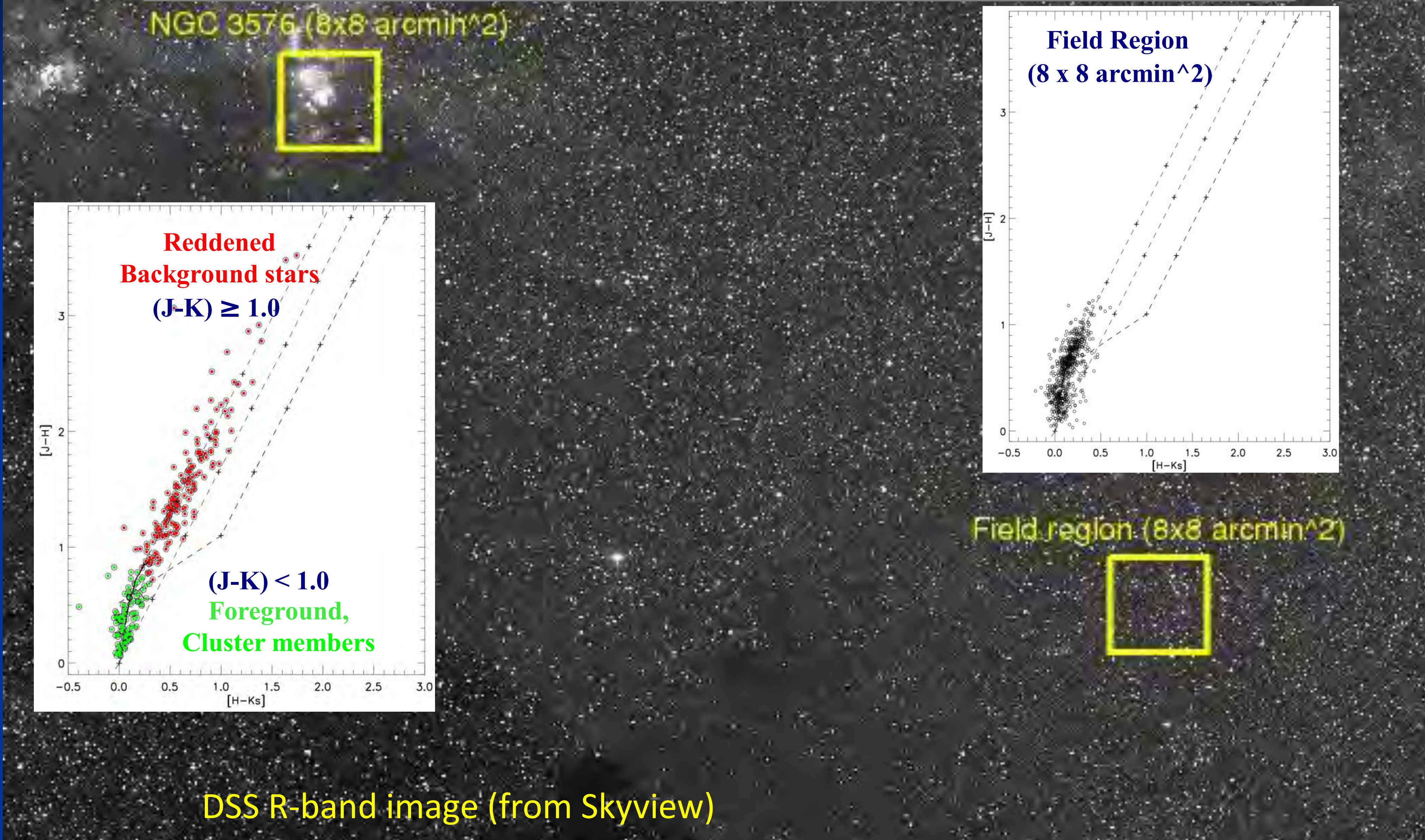

Results: RCW57A

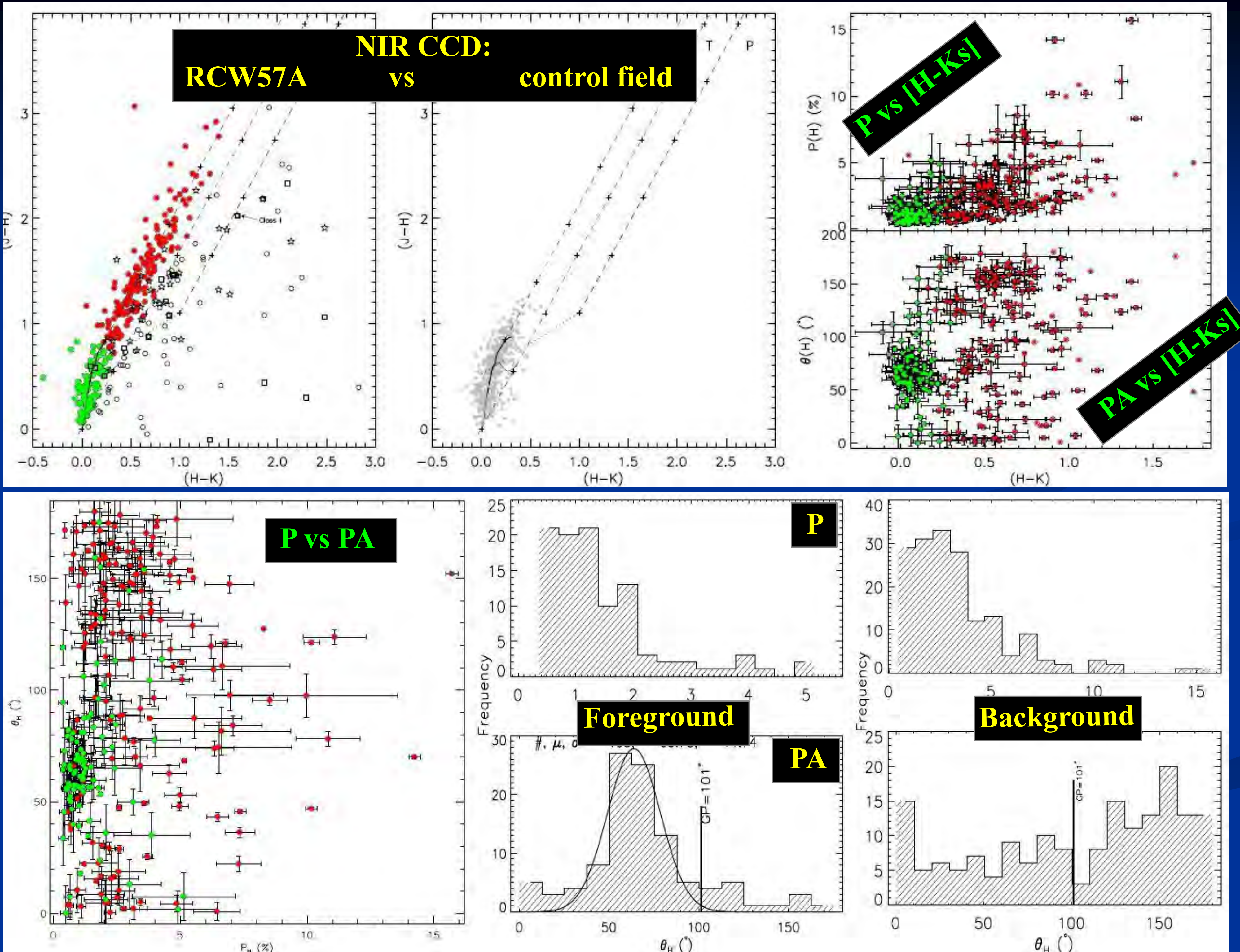

NIR CCD:
RCW57A vs control field
P vs [H-Ks]
PA vs [H-Ks]
P vs PA
P
PA
Foreground
Background
GP=101°
(J−H)
(H−K)
P(H) (%)
θ(H) (°)
Frequency
Class I

Results: RCW57A

Wise 4.6 micron (Red), 2 MASS K-band (green), DSS-II R-band (blue)

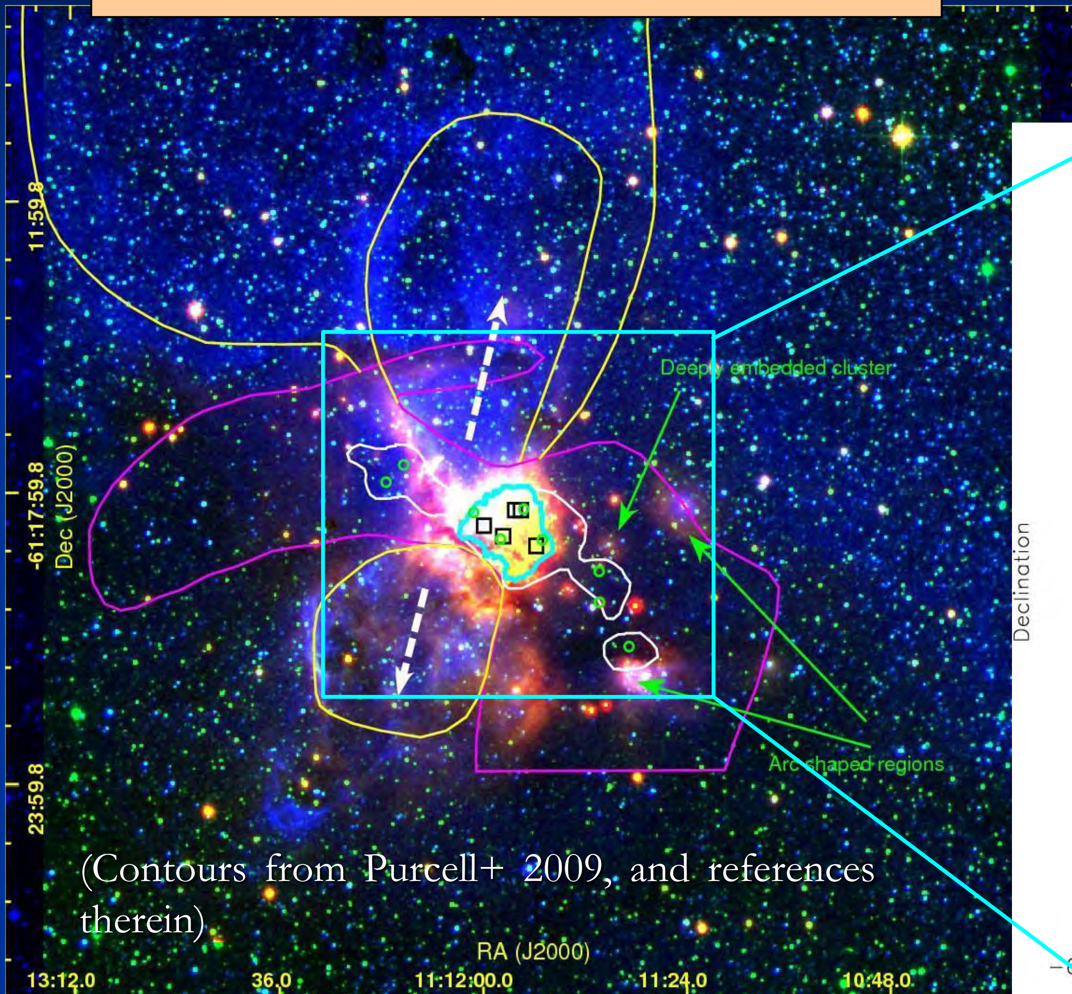

Hour-glass B-field morphology

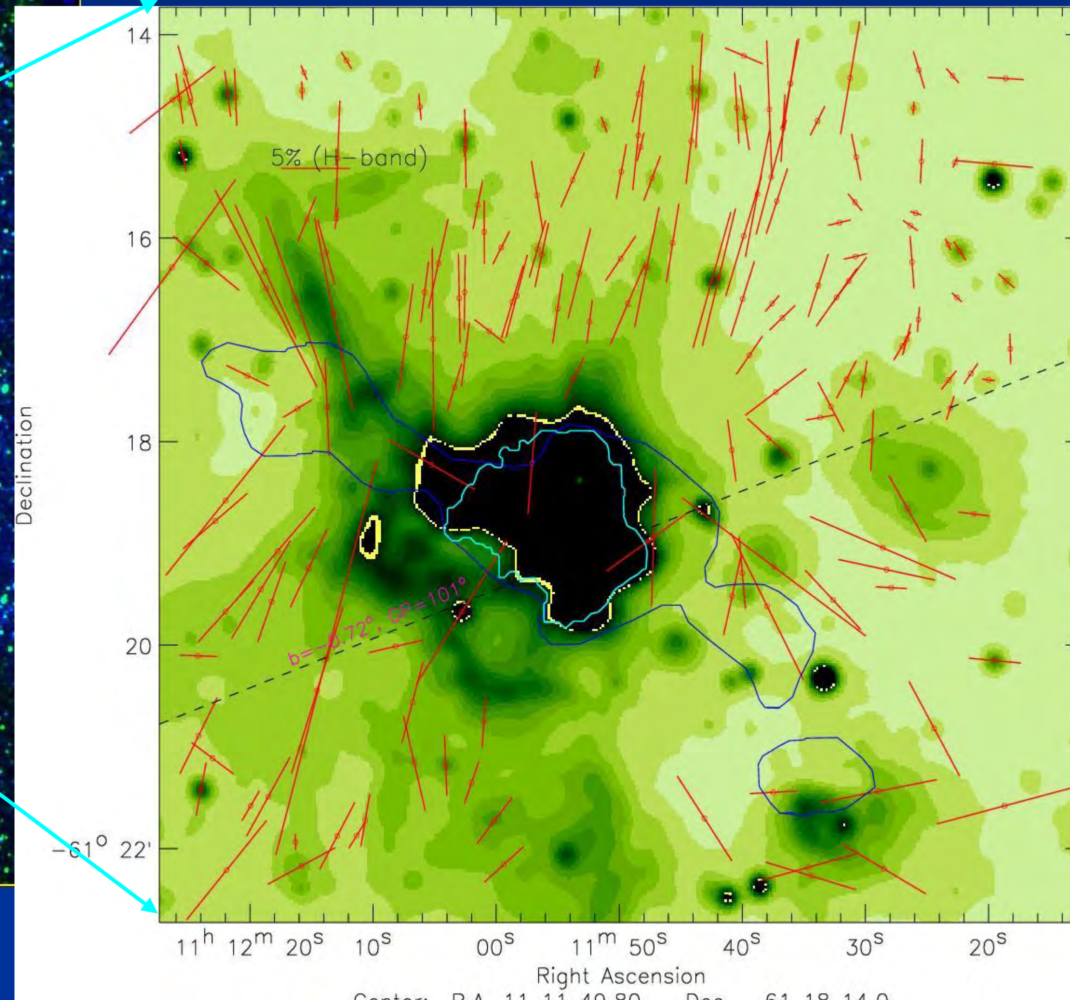

Polarization vector map, using only the probable background stars, plotted on the WISE 12 micron image

Results: RCW57A

Schematic diagram: correlation b/n the structures of sub-mm filament, magnetic fields, bipolar-bubble, and star-formation activity

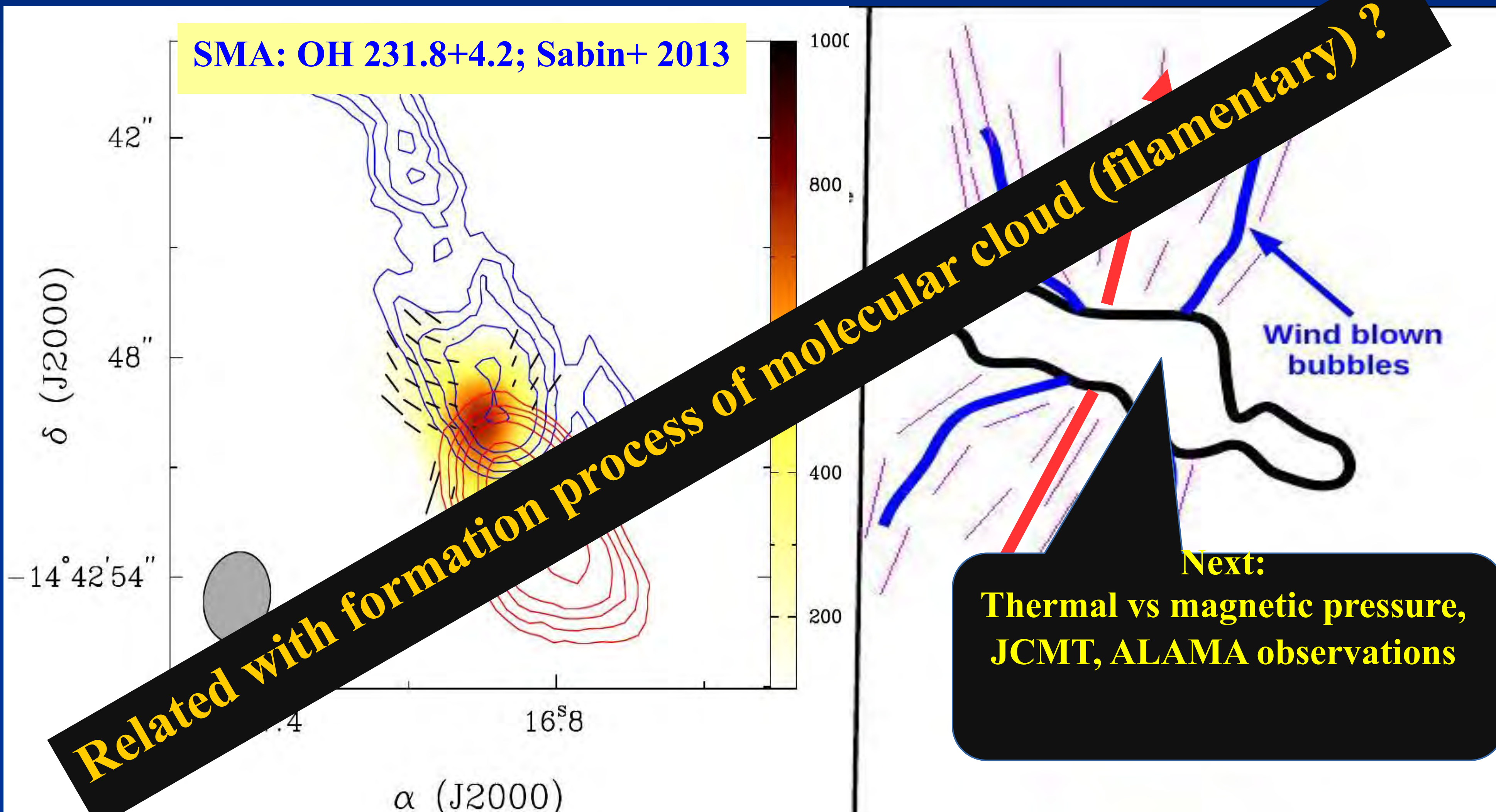

Related with formation process of molecular cloud (filamentary) ?

Next:
Thermal vs magnetic pressure,
JCMT, ALAMA observations

Analogy b/n mid-infrared bipolar bubbles and PPNe? Role of magnetic fields?

NGC 1893 – 3.1 kpc towards anti-center Ga

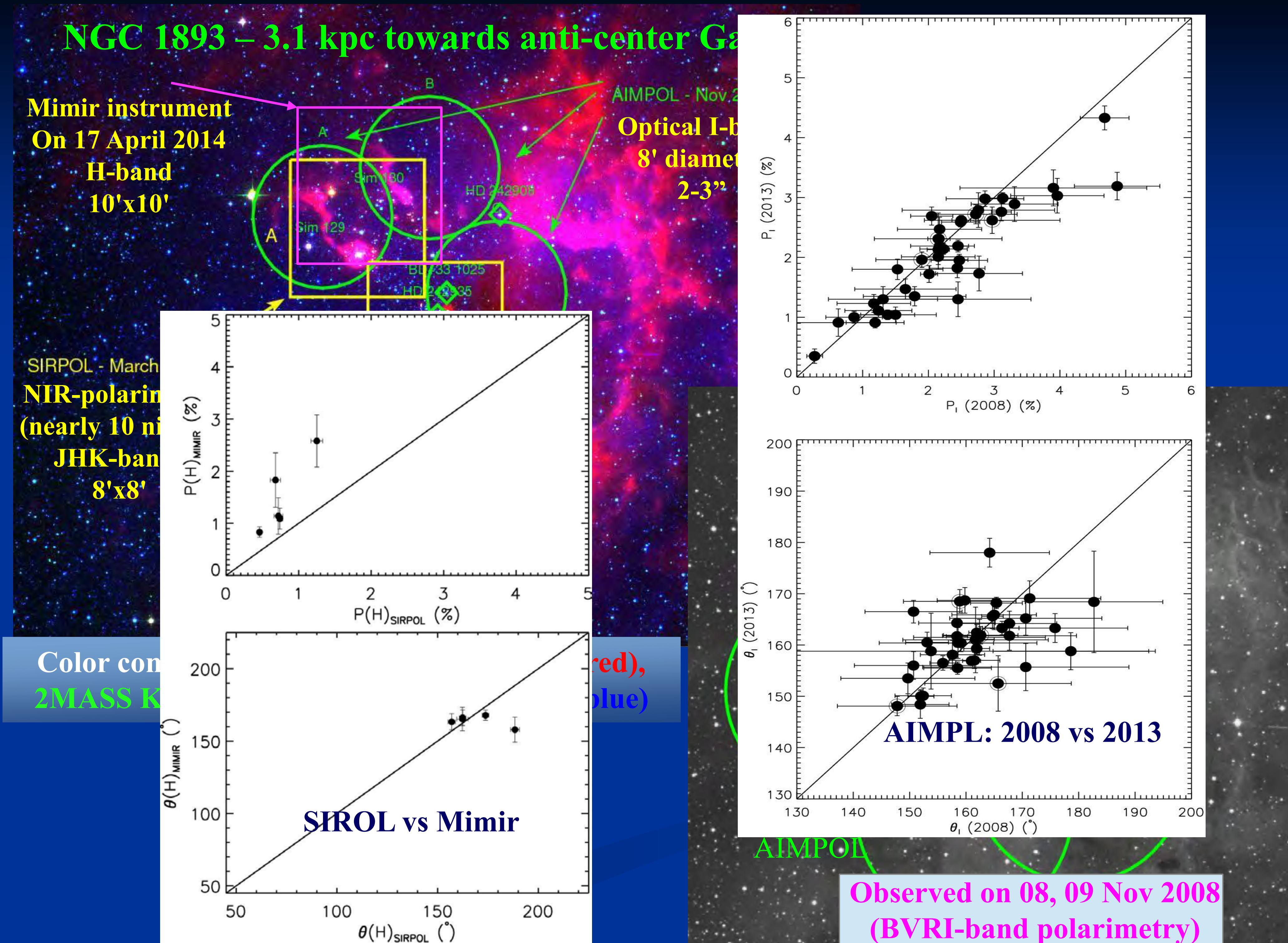

Color con... red), 2MASS K... blue)

Observed on 08, 09 Nov 2008
(BVRI-band polarimetry)

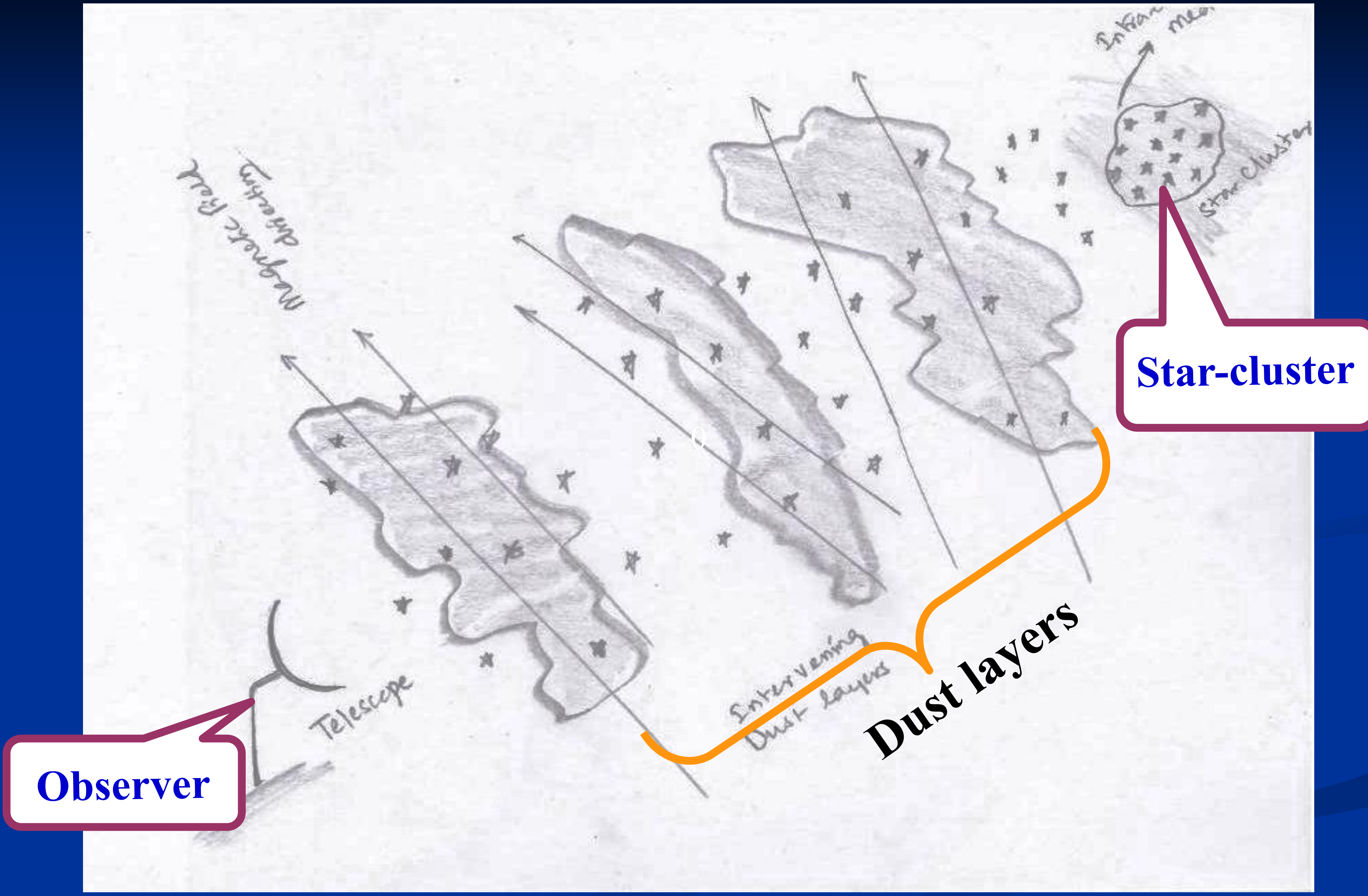

Schematic diagram: polarimetry can traces ISM distribution

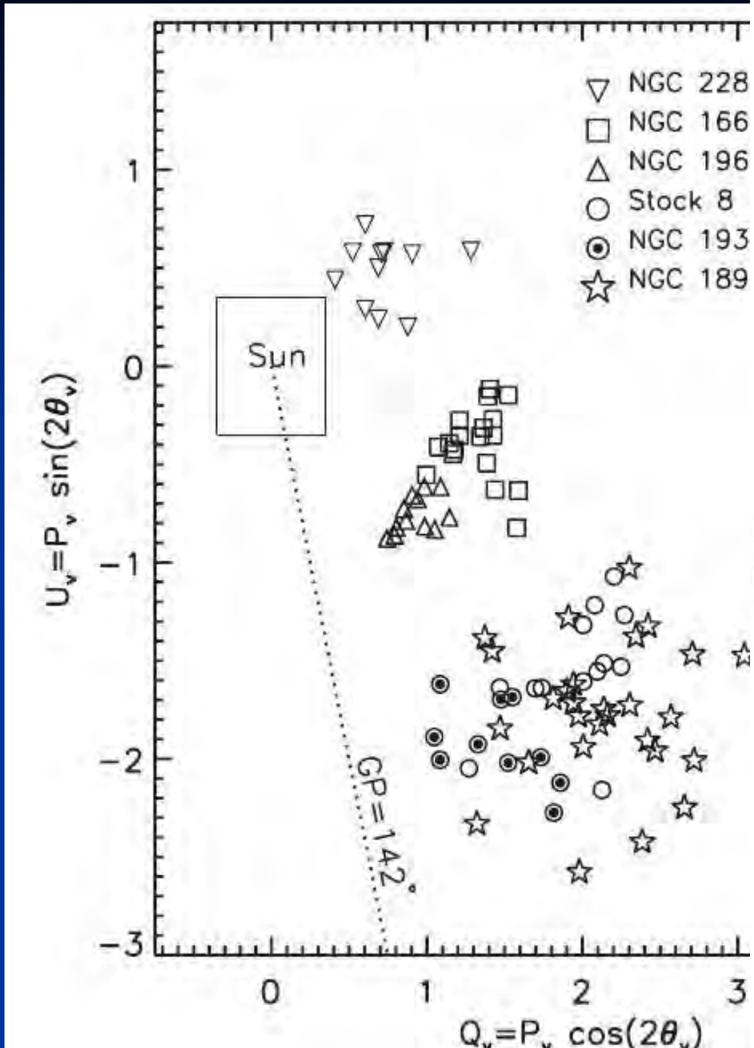

Distribution of Q, U of men
stars of 6 clusters.
Eswaraiah+ 2011
Pandey+ 2013

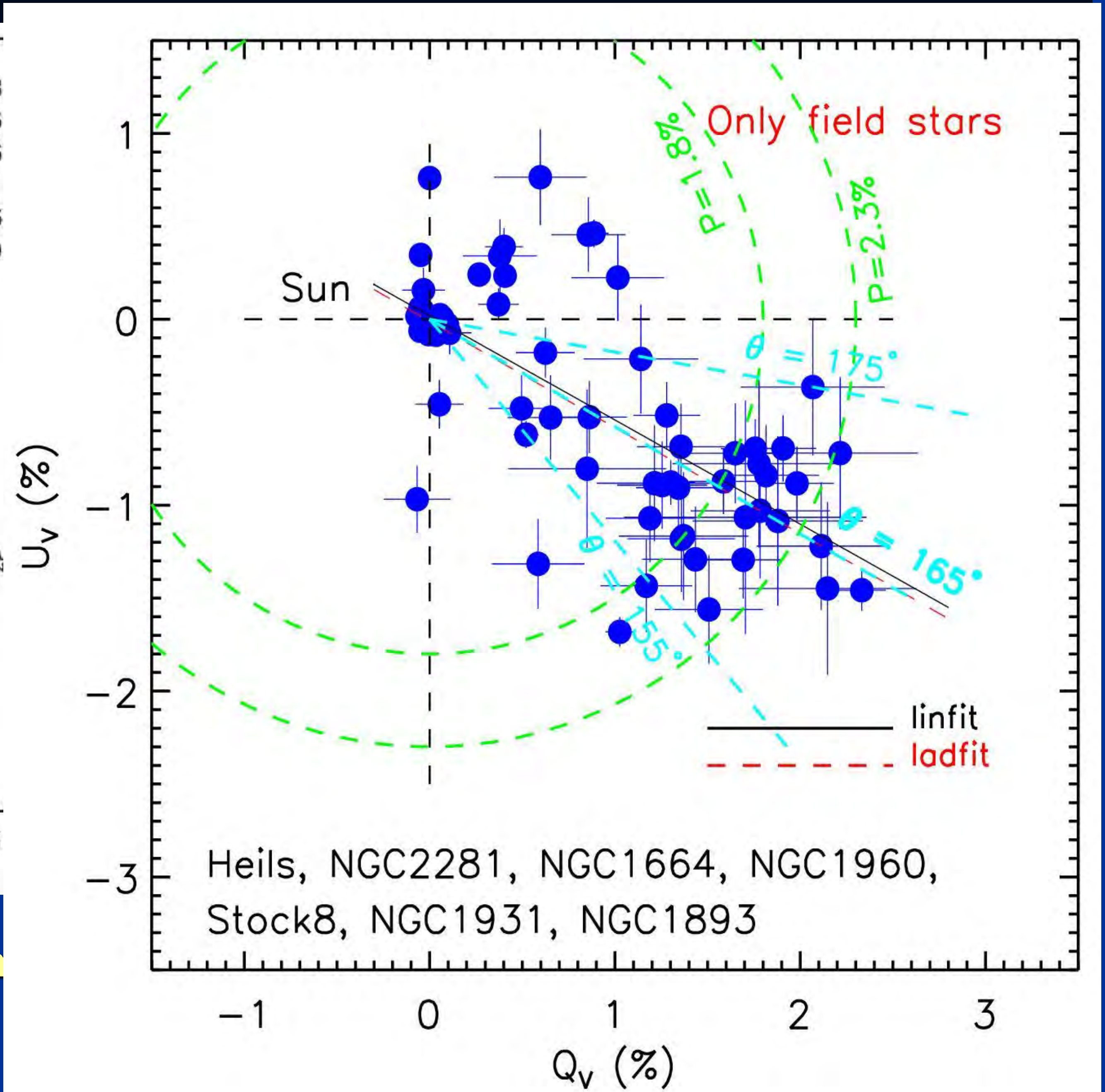

Estimation of foreground polarization
(Eswaraiah+ to be submitted)

Results: NGC 1893

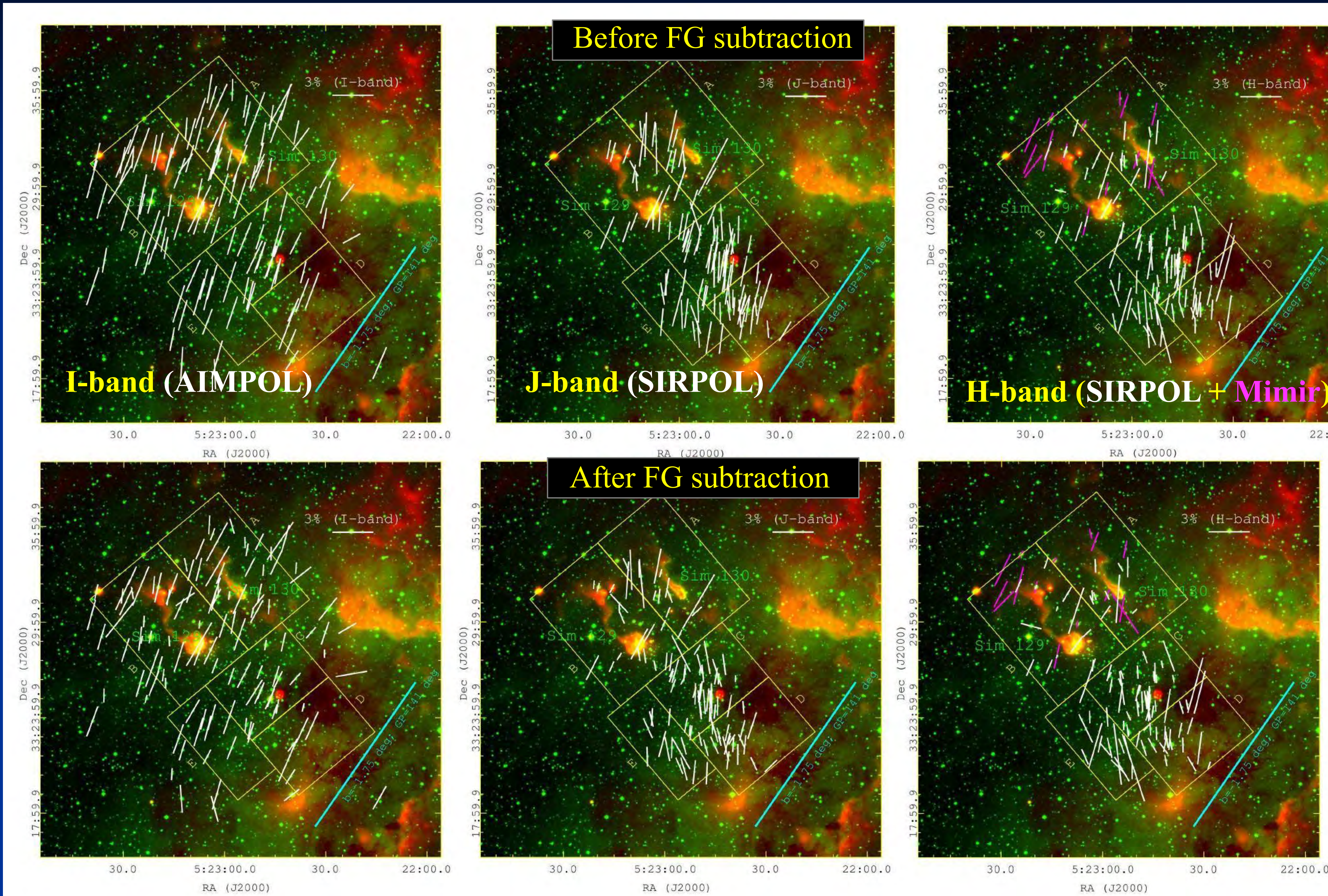

Eswaraiah+
(to be submitted)

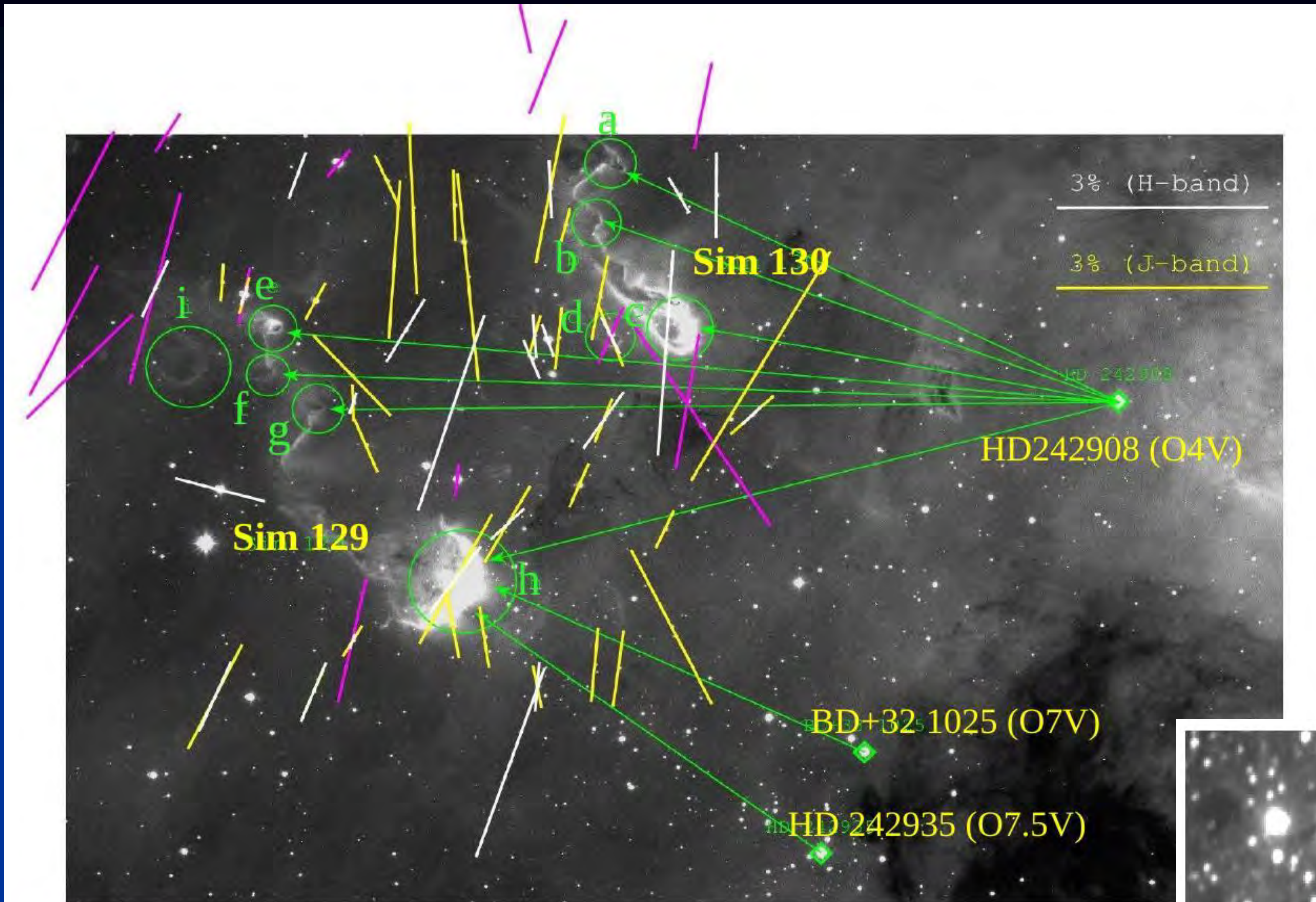

JH-band polarization vectors of 'AB' regions are overplotted on the H_α image (Observations in H_α (Lim et al., 2014) on 2009 January 19 using the AZT-22 1.5 m telescope (f/7.74) at Maidanak Astronomical C Uzbekistan. Thanks to *Lim Beomdu* for kindly providing this image). Red vectors are of J-band (SIRPOL), whi of H-band (SIRPOL), and magenta vectors are of H-band using Mimir instrument. Out of five, three O-type star The probable tiny BRCs are shown with green circles. Most of the tiny BRCs, namely, 'a, b, e, f, g', were belived due to the UV radiation mainly emanating from HD 242908 as their head parts pointing towards HD 242908. The were connected with green arrows from the O-type HD 242908. The other tiny BRCs 'd,i' seem to be pointing O-type stars HD 242935 and BD+33 1025.

B-field structure around Sim 129 and Sim 130 using FG corrected JH-band polarimetry - on Hα image (Thanks to Lim+ 2014)

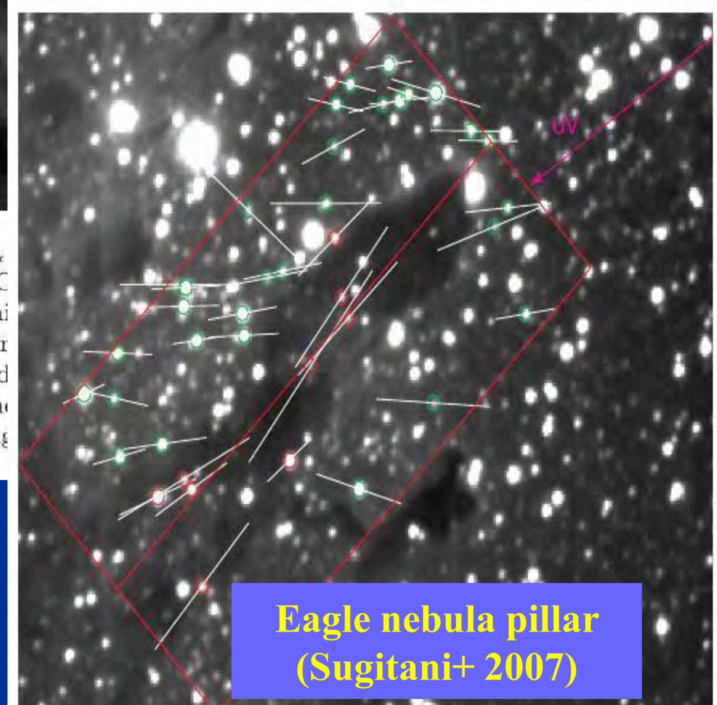

Eagle nebula pillar (Sugitani+ 2007)

Strong vs weak fields

- Weakly magnetized globules with initial field strength of 59 μG evolved similar to hydrodynamic case, strongly magnetized (~ 186 μG) clumps evolved in a different way – 3D simulations by Henney et al. (2007).

- Strong magnetic fields – drastically changes the evolution of I-front, -- structure, compression, flow of ionized gas from the I-front were strongly constrained .

- Strong fields perpendicular to the radiation front: Ionized gas confined to a dense ribbon, or filament stand-off from the globule – which shields the globule from the ionizing radiation (Henny et al. 2007).

- Weak fields oriented perpendicular to the radiation propagation initially, magnetic fields were swept into alignment with the pillar/globule during later evolutionary stages. (Henny et al. 2007, Macky & Lim 2011, 2013)

Cep OB3 (LDN 1225)

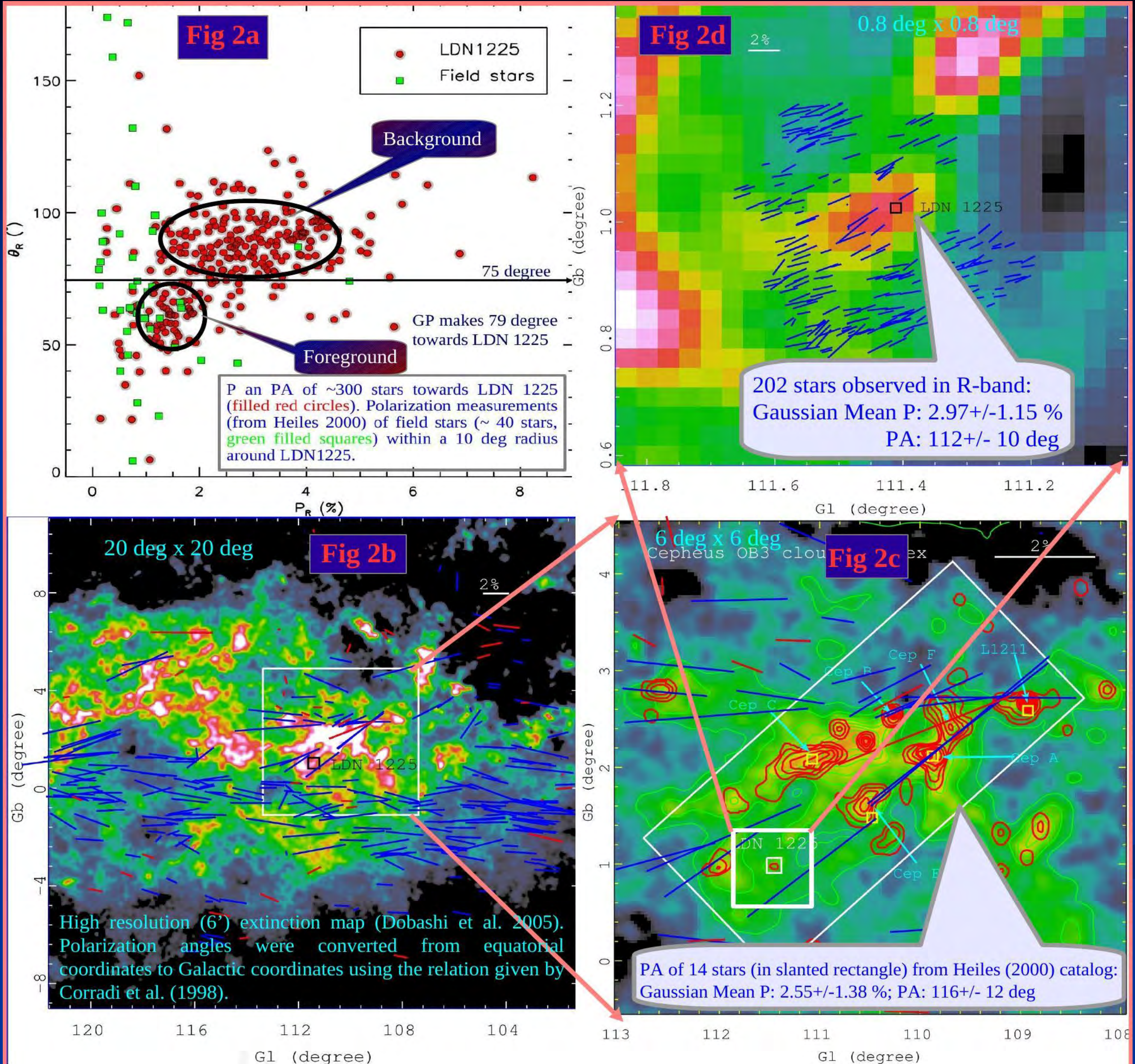

Summary

RCW57A/NGC3576: Hour-glass morphology, role in the formation of filamentary cloud, and collapsing cloud, guided the direction and propagation of the bubble, and its further expansion into the ambient medium. Further sub-mm polarimetry with JCMT, SMA, ALMA of filament will be more useful.

[Eswaraiah, Chen+ in prep]

NGC1893: Optical and NIR-polarimetry, FG contribution, field geometry of two elephant trunks Sim 129 and 130: difference either in the magnetic field strengths or difference in the impact of I-front, relatively bigger dust grains in NGC 1893.

[Eswaraiah, Chen+ to be submitted]

CephOB3 cloud complex: Coherent magnetic fields - larger (Cepheus OB3 cloud complex) to smaller scales (LDN 1225). filament vs B-field orientation, out flow from CepA HW2 aligned with ambient magnetic fields. Planned - further for optical and NIR-polarimetry of entire cloud region.

[Eswaraiah, Chen+ in prep]

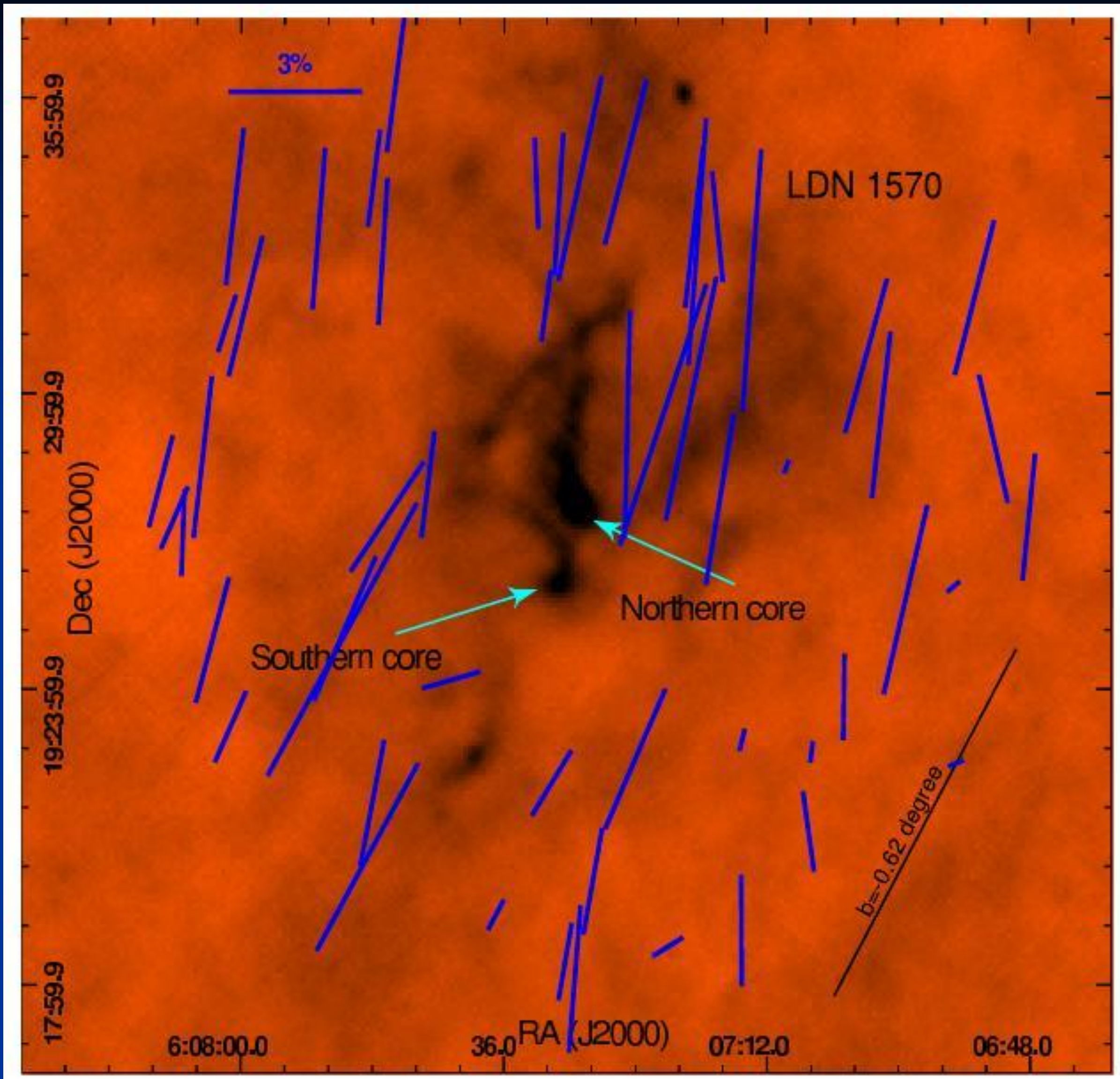

The polarization vectors (blue) of 54 stars that are distributed in a 10 arcmin radius around the cloud center are over-plotted on false color image of Herschel 250 micron SPIRE (Griffin et al., 2010) Photometer Short (250µm) Wavelength Array (PSW) of the field containing L1570.

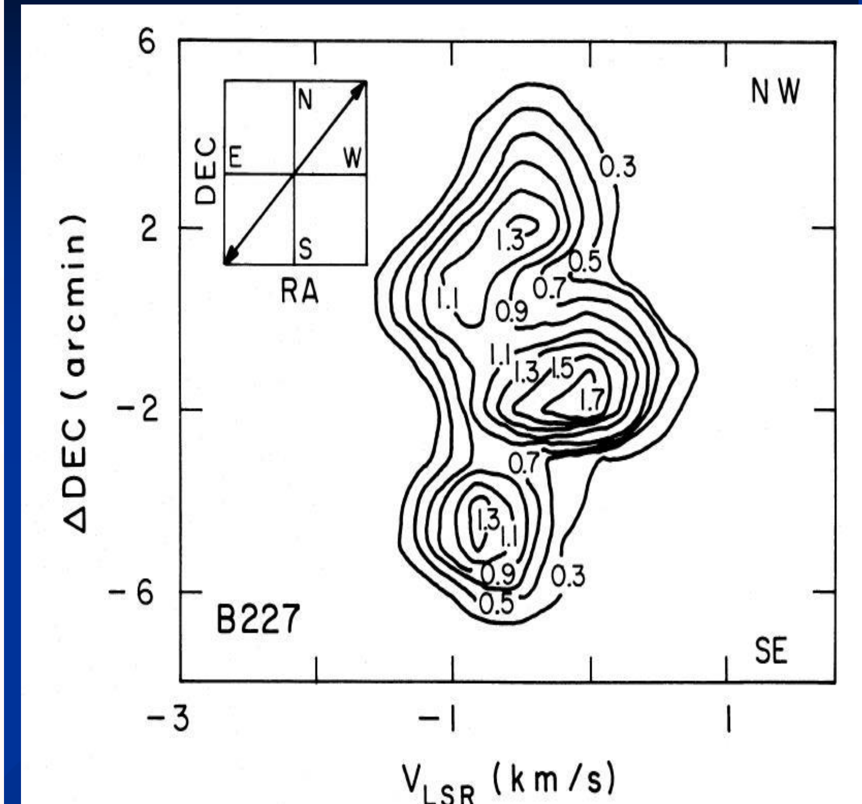

13CO spatial velocity diagram along NW (Arquilla & Goldsmith 1986) direction. Largest (0.5 km/s) velocity shifts have been observed along the line joining the major sub-condensations (Arquilla & Goldsmith 1985).

LDN1570/Barnard 227
(Eswaraiah+ 2013)

FG dust layers towards NGC 1893

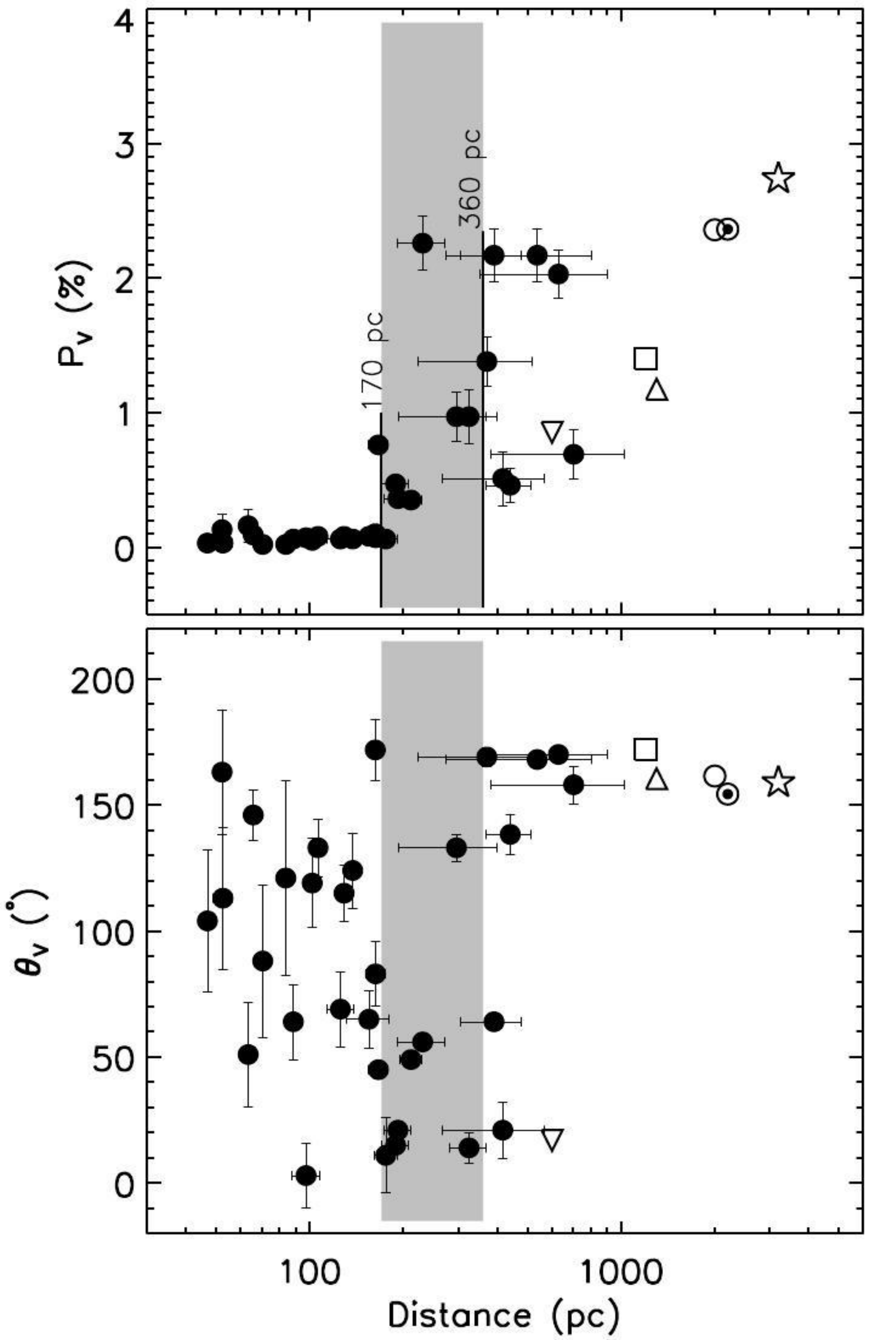

NGC1893
(Eswaraiah+ 2011);
NGC 1931 (Pandey+ 2013)

05h 46m, +28d 56 arcmin

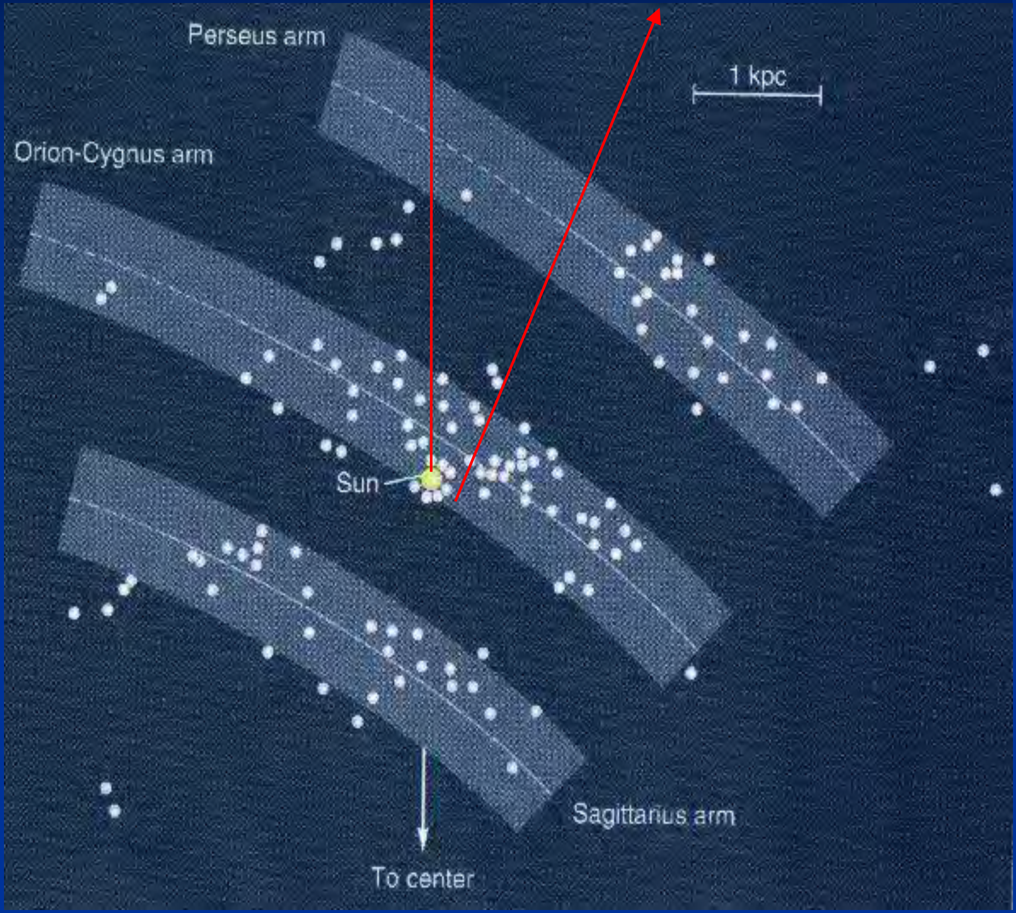

17h 46m ; -29d 0.5 arcmin

Heiles (2000) catalogue
Distances from Hipparcos the New Reduction catalogue (van Leeuwen, 2007)

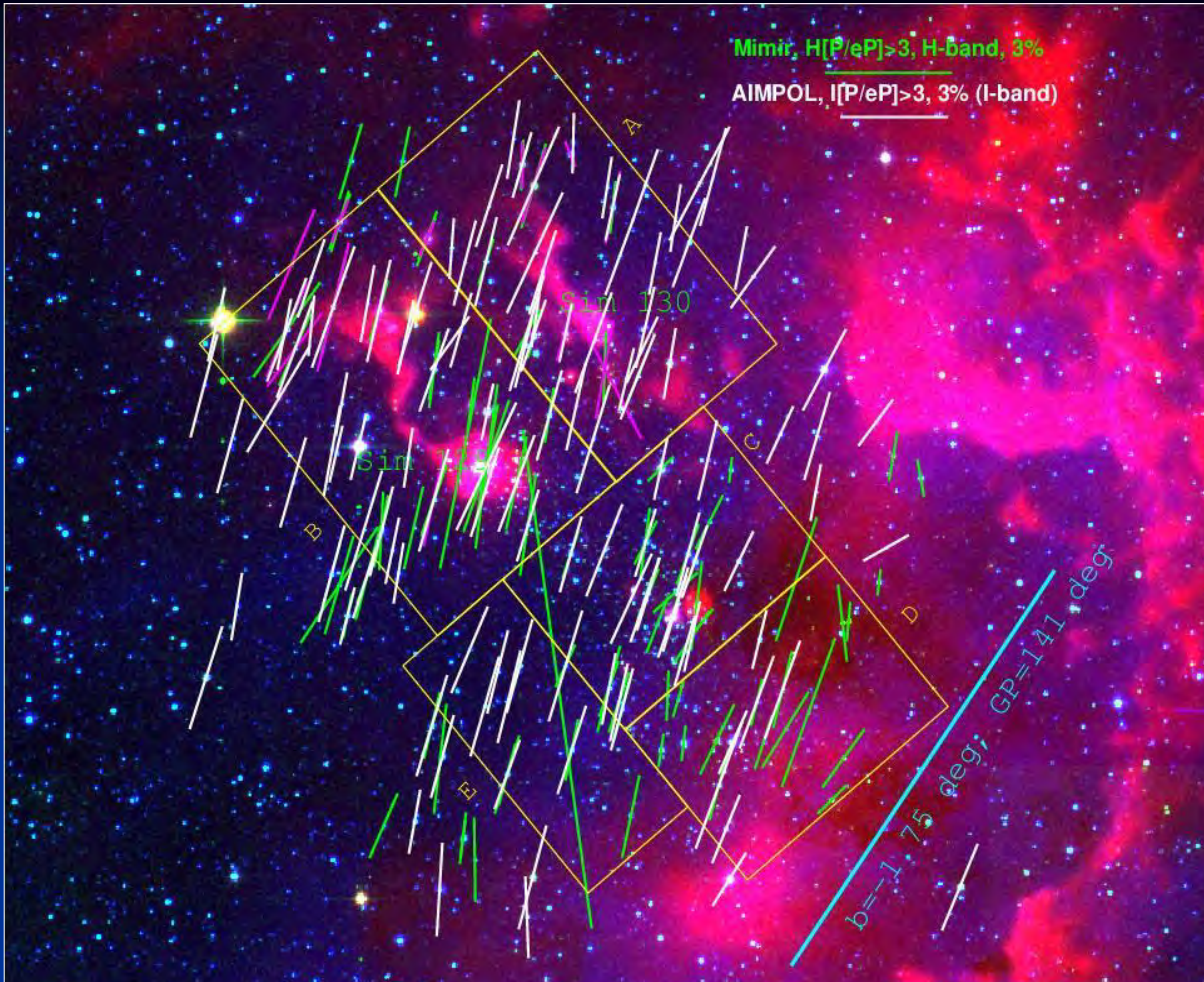

Mimir, H[P/eP]>3, H-band, 3%
AIMPOL, I[P/eP]>3, 3% (I-band)
A
B
C
D
E
Sim 130
Sim 129
b=-1.75 deg; GP=141 deg

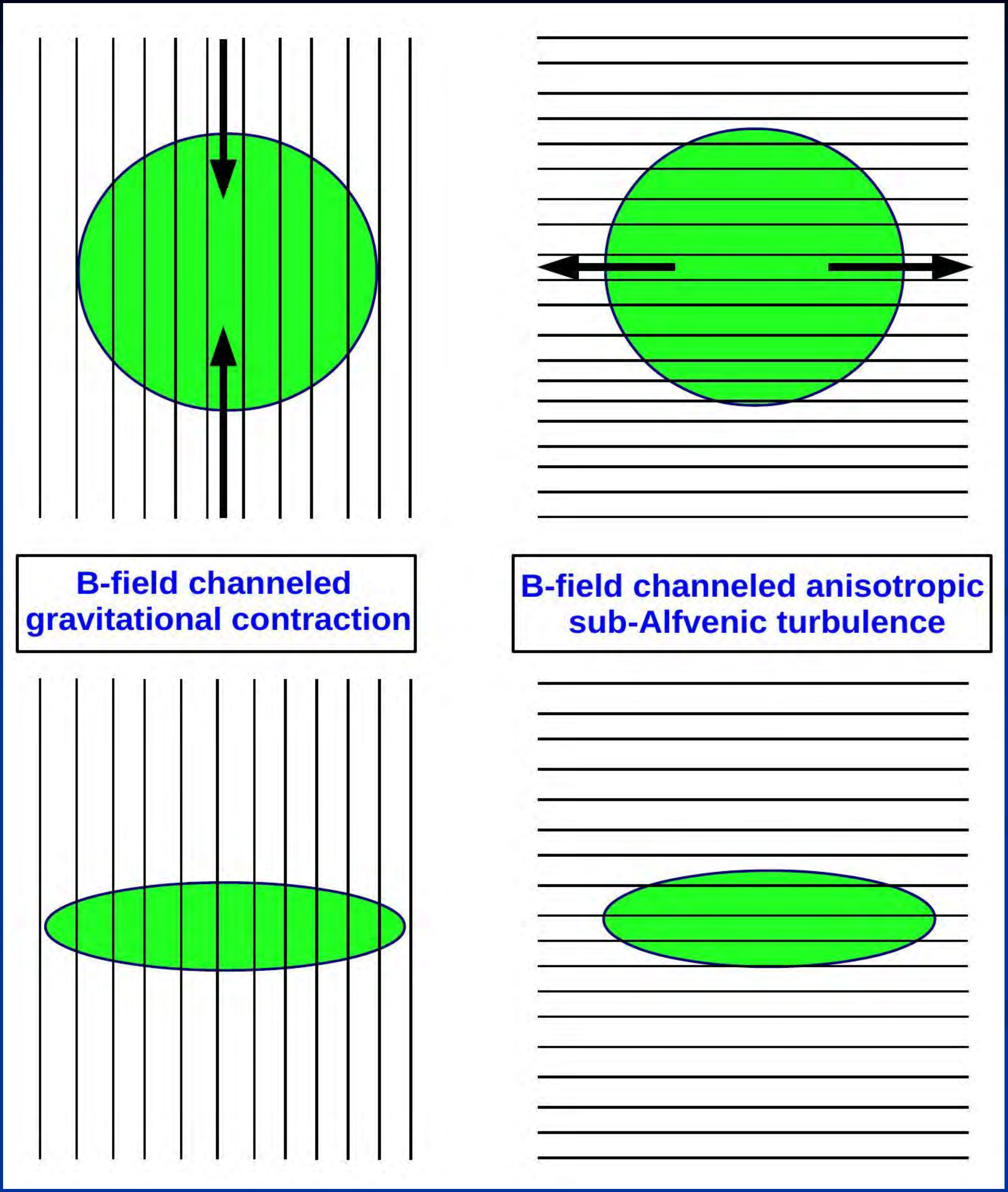
B-field channeled
gravitational contraction
B-field channeled anisotropic
sub-Alfvenic turbulence

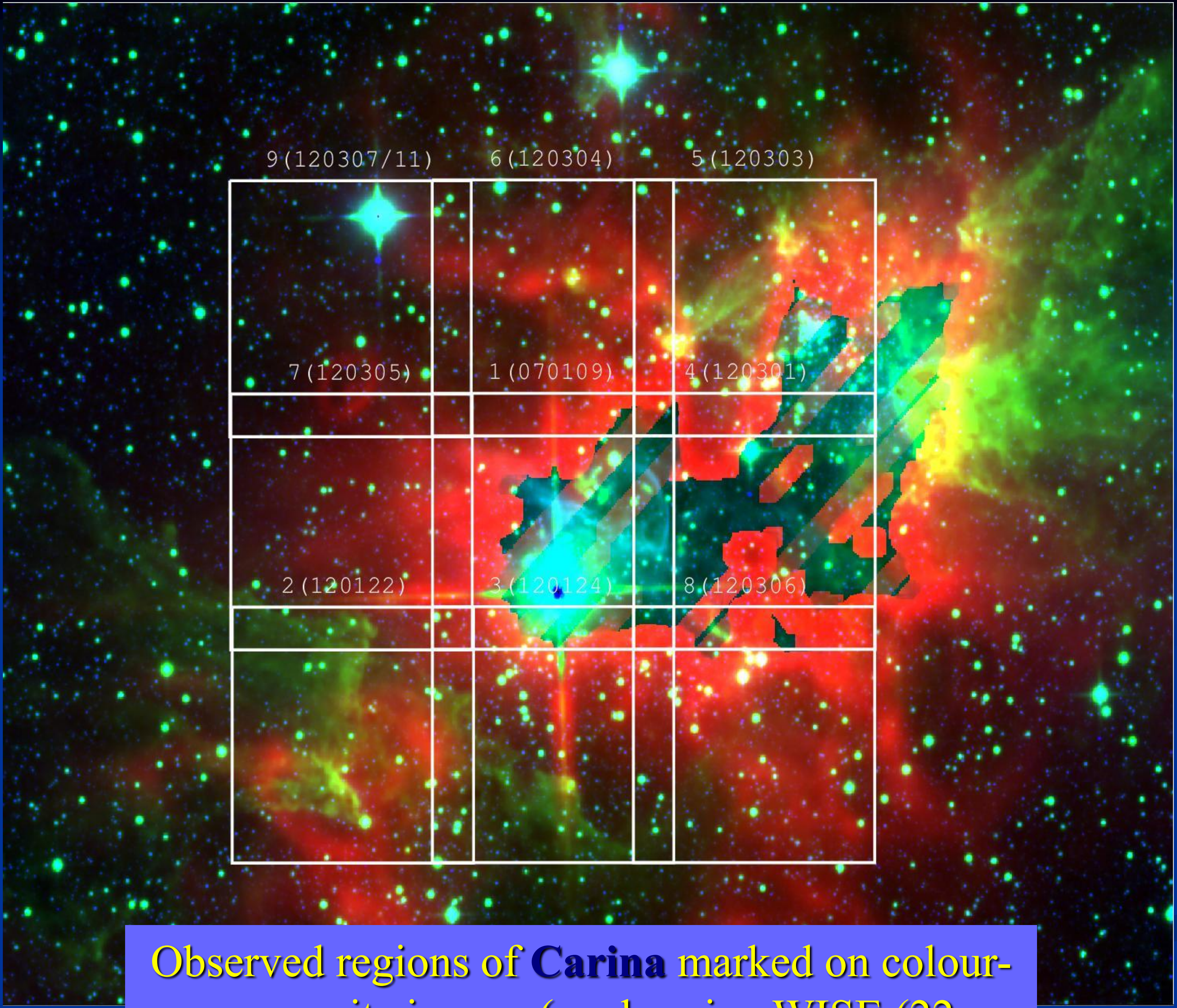

Observed regions of **Carina** marked on colour-composite image (made using WISE (22 micron, 4.6 micron) and 2MASS K-band image

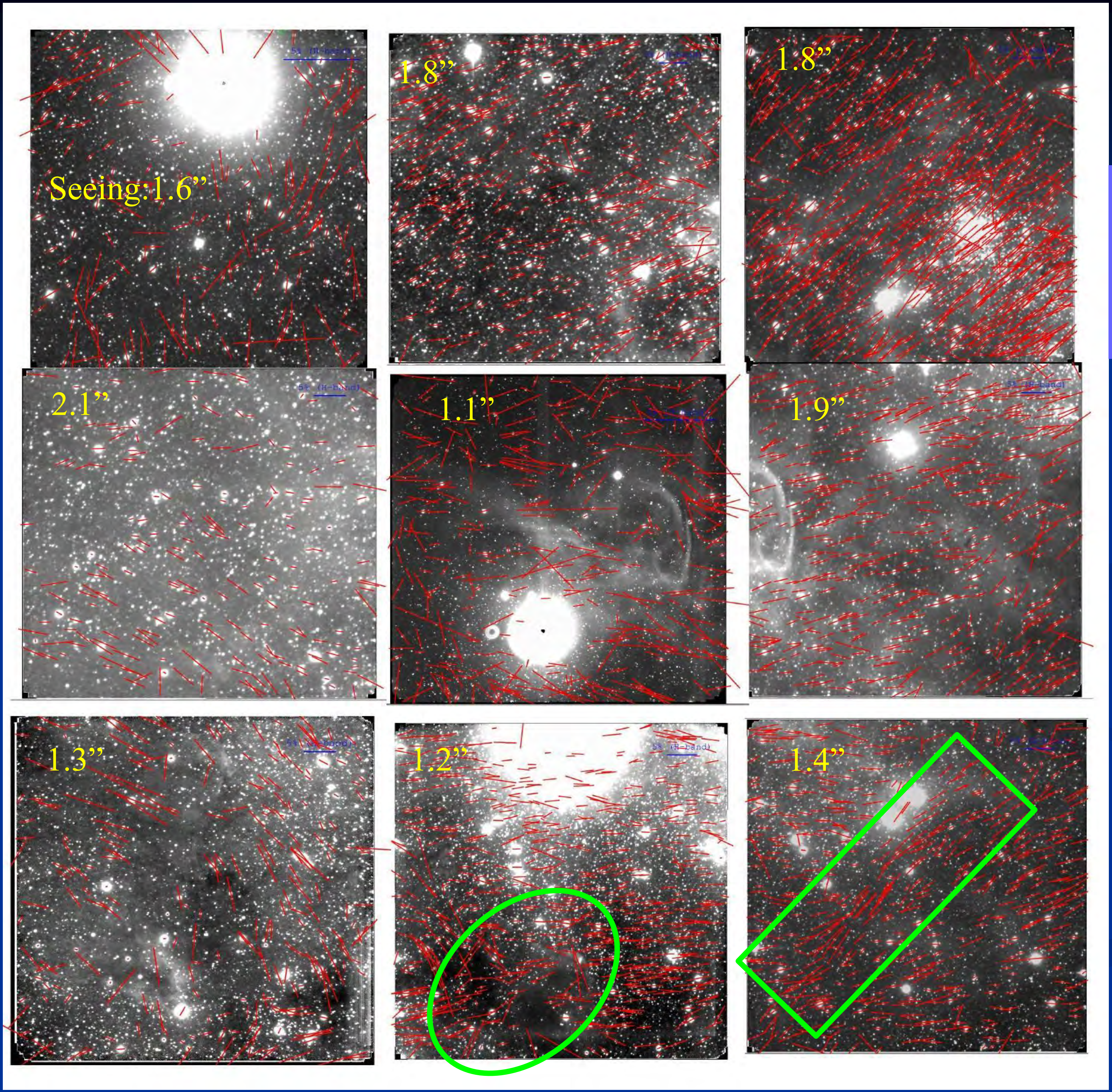

H-band polarization vectors of 9 fields towards Carina

1) In some cases: stars in common fields were not matching

2) Further analysis: identification - YSOs, foreground, background stars

3) Mosaic image

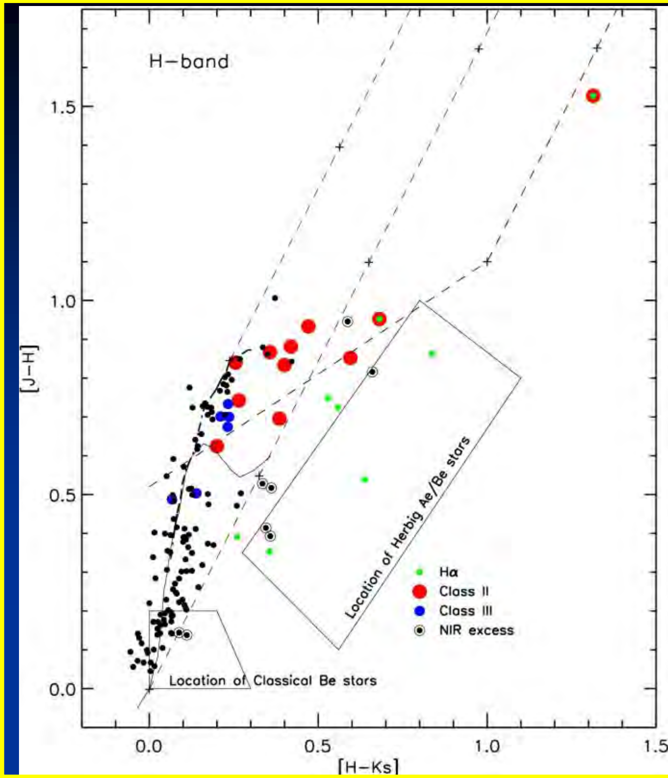

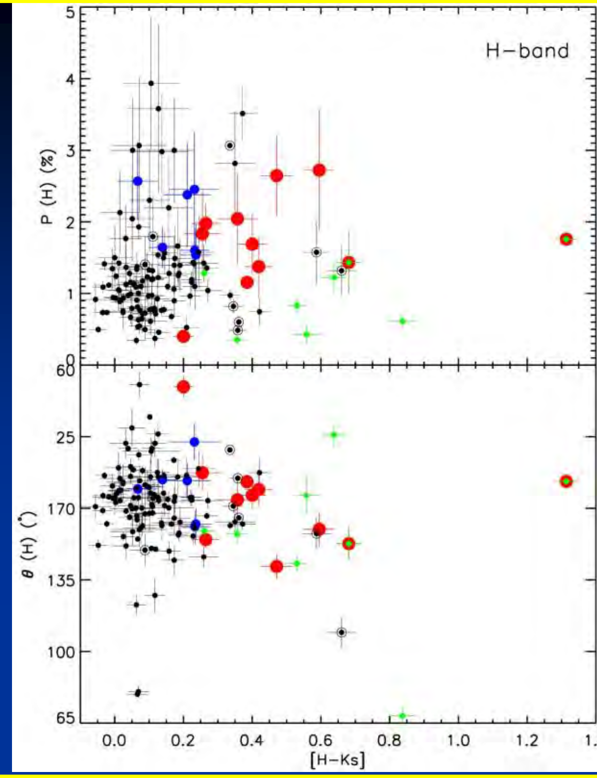

* NIR color-color diagrams were used to identify the YSOs, and were excluded.

* P vs [H-Ks] – dichroic origin of polarization.

* Halpha, Class II, Class III, and other NIR excess stars – identified – using literature

* Measurements of known foreground non-member – used to estimate FG contribution.

* FG medium - characterized – mean size dust grains – uniform B-field component.

* FG corrected, intra-cluster medium found to have relatively bigger dust grains.

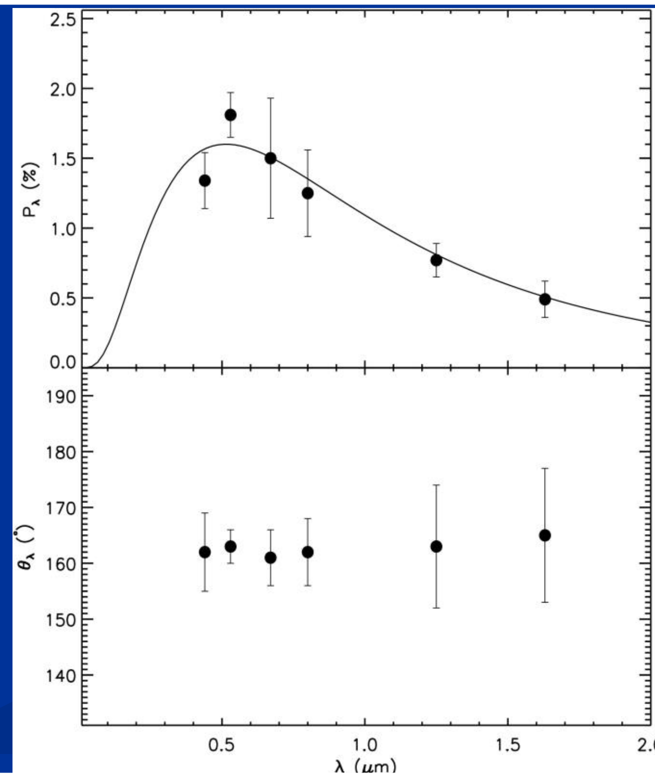

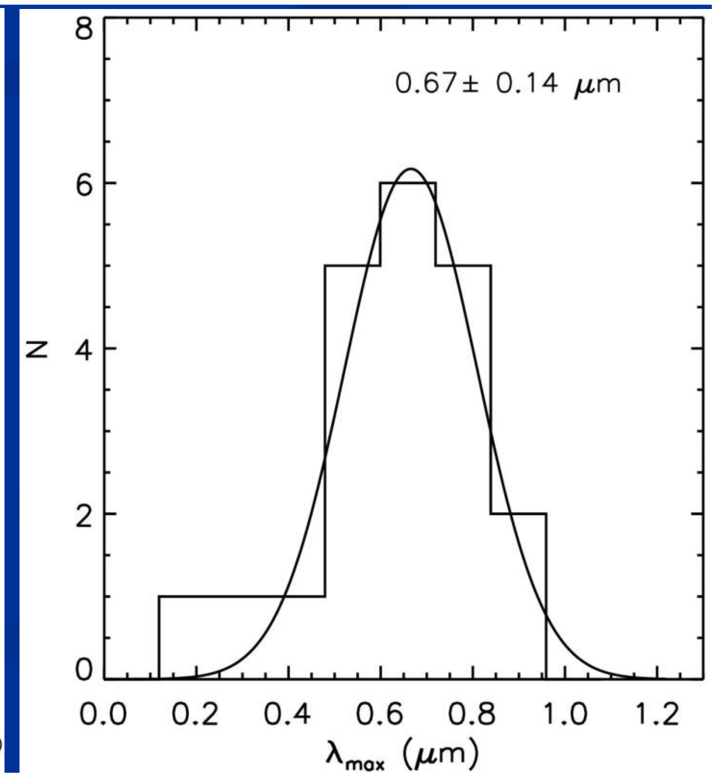

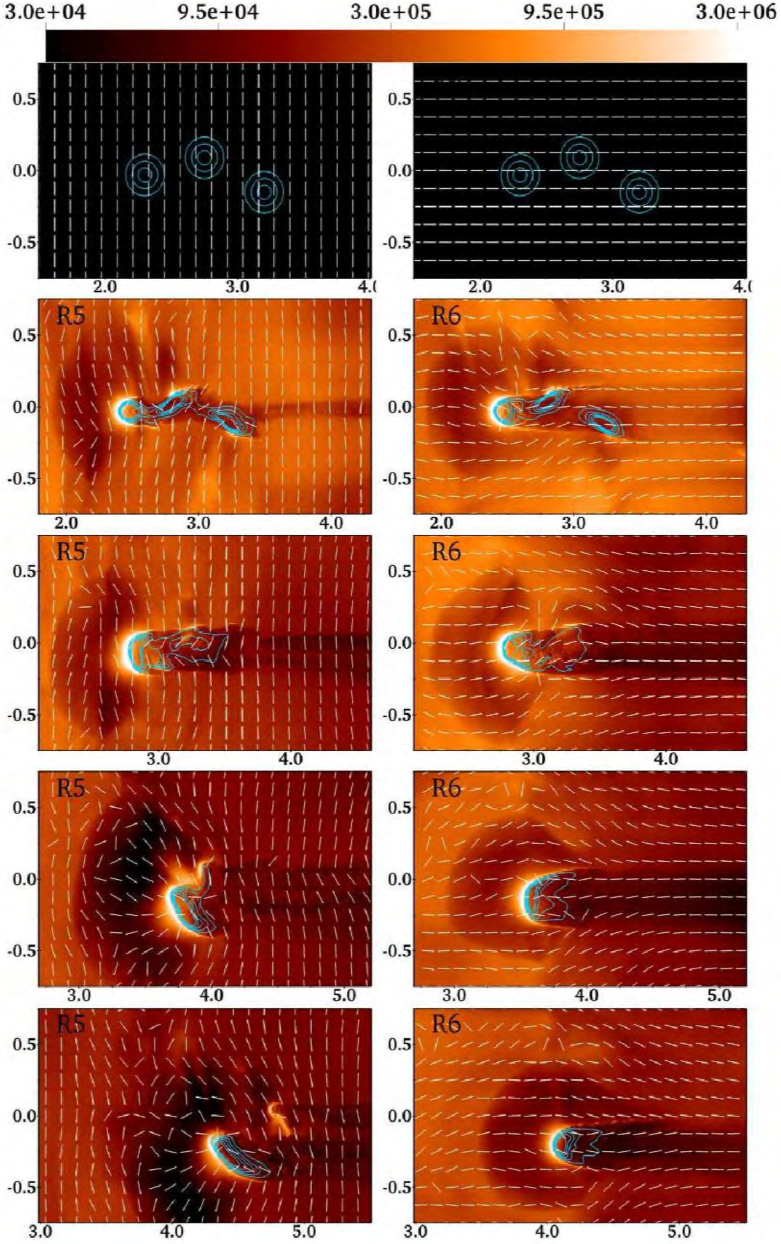

Figure 1: Projections through Simulations R5 (left) and R6 (right) at times (from top to bottom) 0, 100, 200, 400, 500 kyr. The image x- and y-axes are the simulation x- and z-axes; the line of sight is the simulation y-axis. The colour scale shows Hα intensity, integrated along the line of sight assuming no background sources. White lines indicate projected magnetic field orientation at the midpoint of each line, and turquoise contours show projected neutral hydrogen density on a linear scale. The five contours are at $N(H^0) = (0.2, 0.4, 0.6, 0.8, 1.0) \times 10^{21}$ cm^{-2}. Positions are shown on the axes labels in parsecs relative to the source; not all of the simulation is shown, and the image window moves further from the source from image to image.

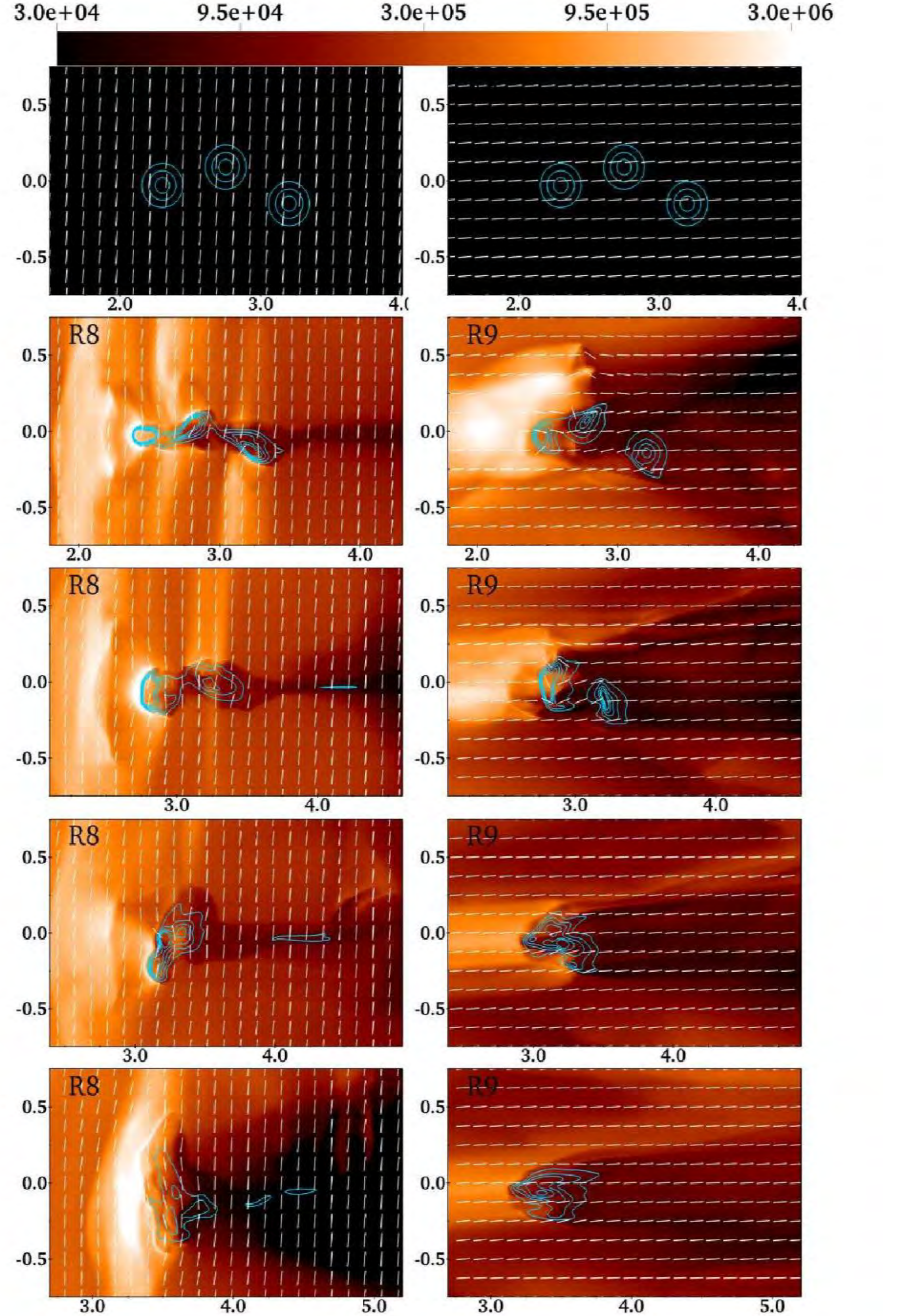

Figure 2: As Fig. 1 but showing projections through simulations R8 (left) and R9 (right) at times (from top to bottom) 0, 100, 200, 300, 400 kyr. The projection and the colour scales are the same as before.

Mackey & Lim 2011

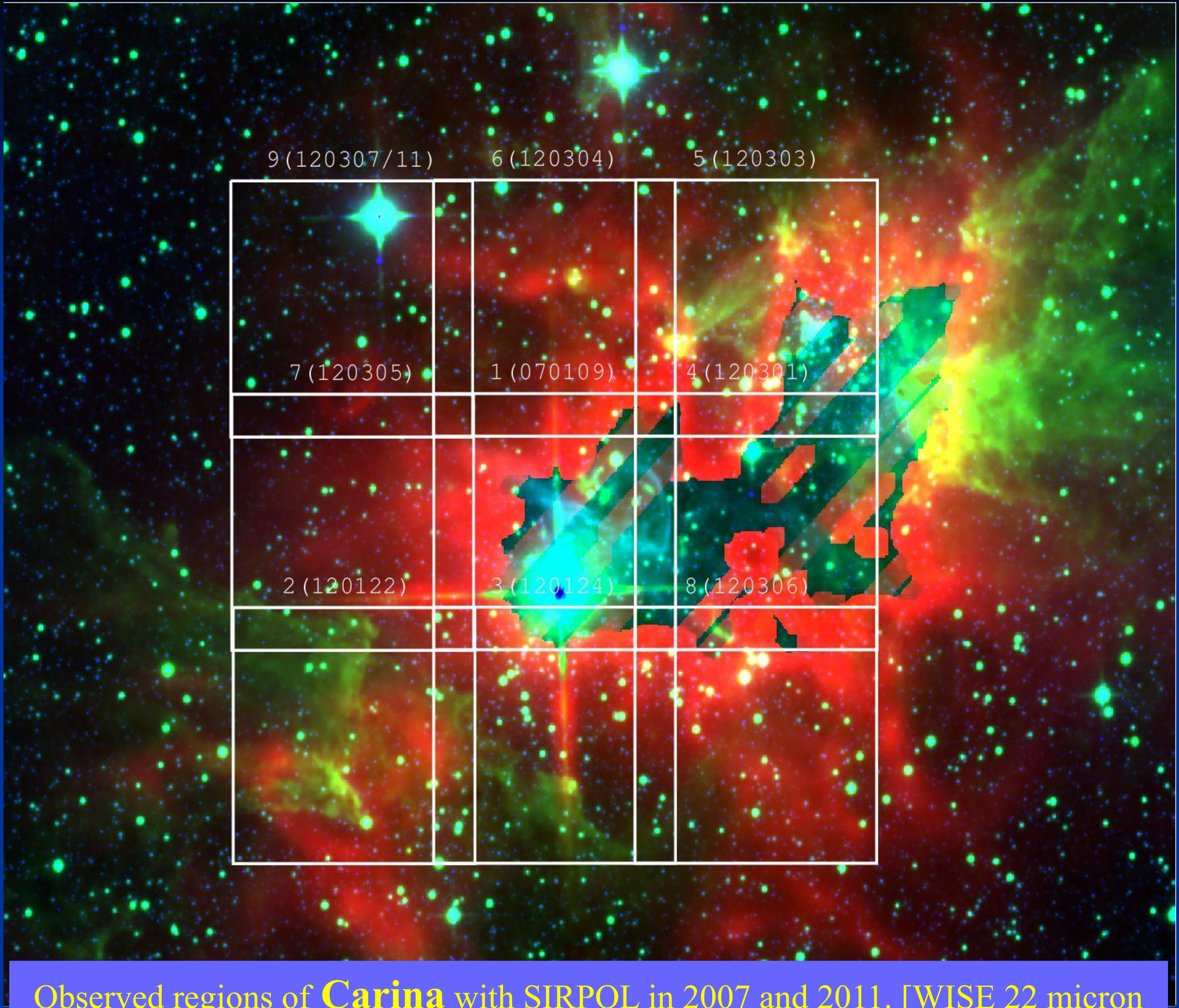

Observed regions of **Carina** with SIRPOL in 2007 and 2011. [WISE 22 micron (red), WISE 4.6 micron (green) and 2MASS K-band (blue) images]

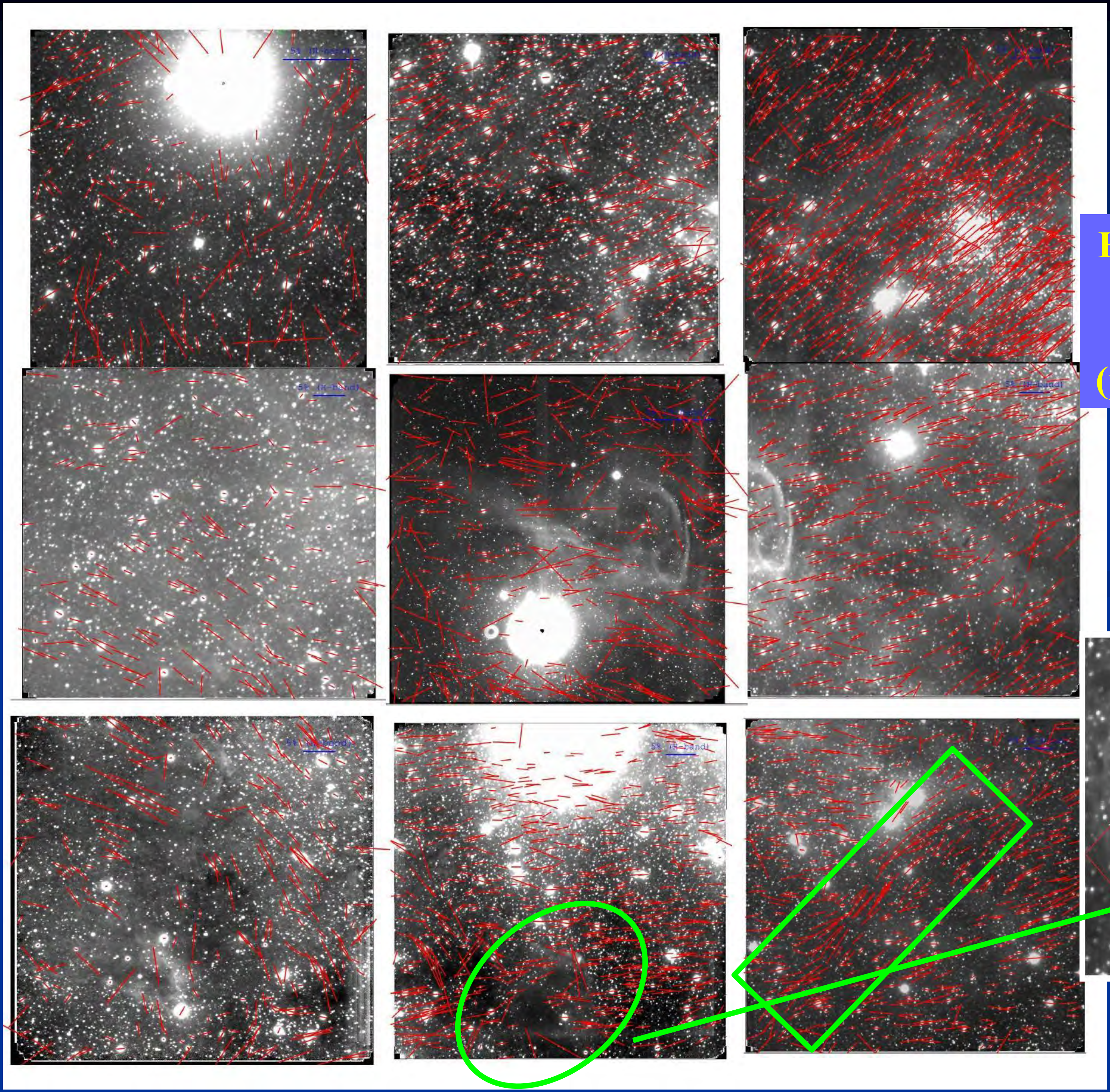

H-band polarization vectors of 9 fields towards Carina (preliminary results)

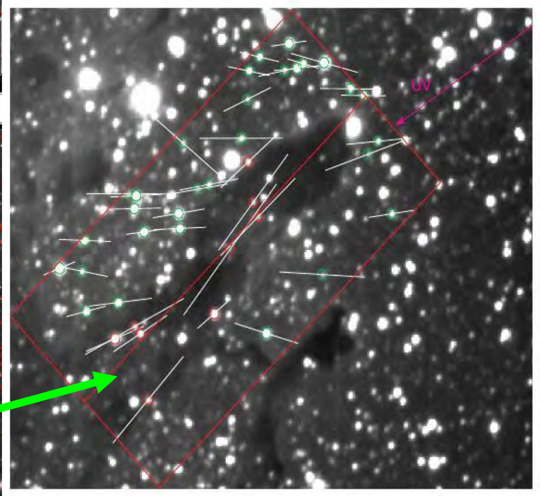

Eagle nebula pillar (Sugitani+ 2007)

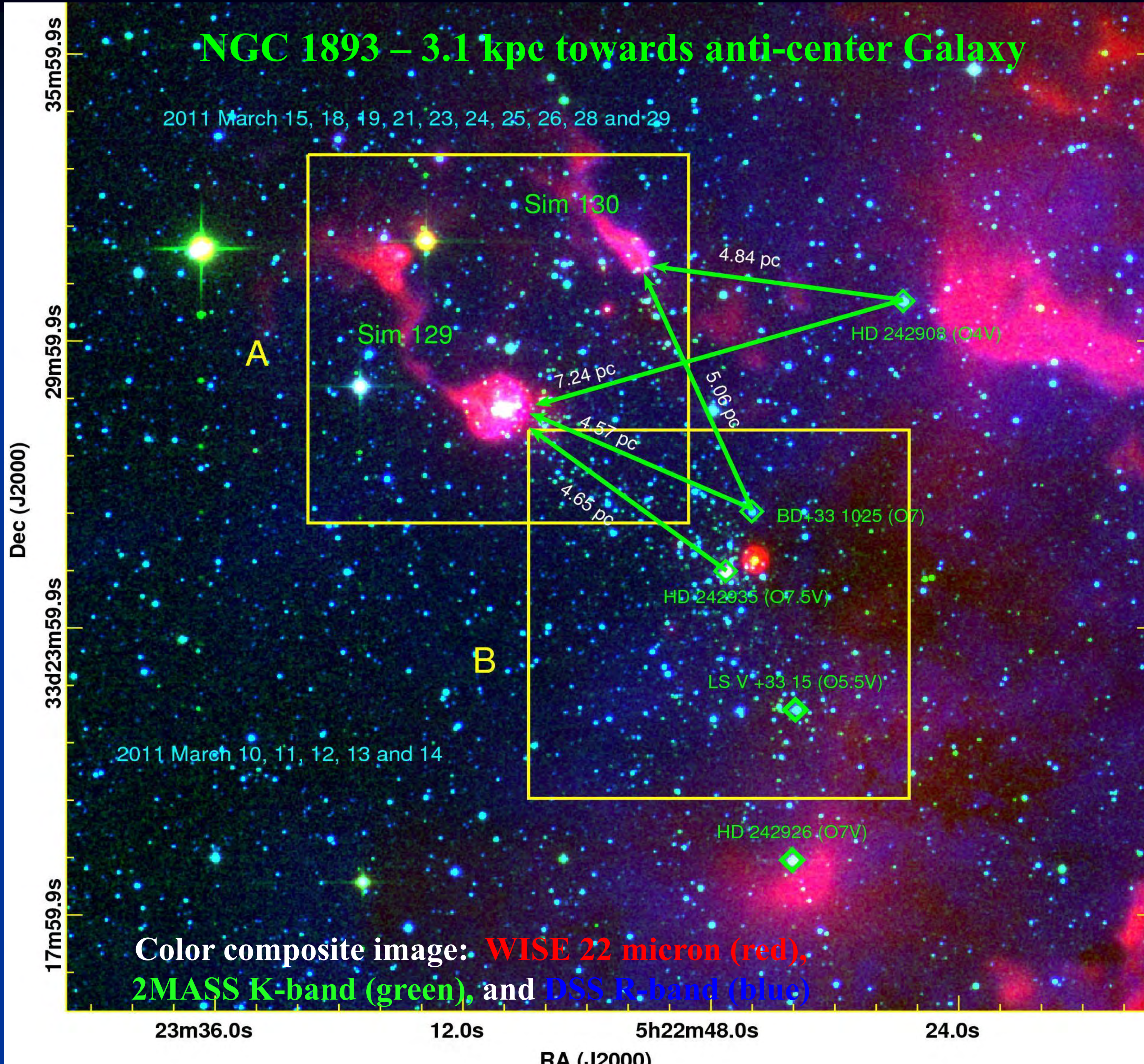

NGC 1893 – 3.1 kpc towards anti-center Galaxy
2011 March 15, 18, 19, 21, 23, 24, 25, 26, 28 and 29
Sim 130
Sim 129
A
4.84 pc
HD 242908 (O4V)
7.24 pc
5.06 pc
4.57 pc
4.65 pc
BD+33 1025 (O7)
HD 242935 (O7.5V)
B
LS V +33 15 (O5.5V)
2011 March 10, 11, 12, 13 and 14
HD 242926 (O7V)
Color composite image: WISE 22 micron (red),
2MASS K-band (green), and DSS R-band (blue)
35m59.9s
29m59.9s
33d23m59.9s
17m59.9s
Dec (J2000)
23m36.0s
12.0s
5h22m48.0s
24.0s
RA (J2000)

THANK YOU VERY MUCH
FOR YOUR KIND ATTENTION

Summary: RCW57A

- **Magnetic fields are found to be very important in guiding the expansion of I-front from the embedded young O/B stars in side RCW57A**
- **Filamentary clouds cloud have been formed due to compression of material along the field lines.**
- **Fields lines could have acquired hour-glass morphology when clouds tends to contract inward and collapse**
- **Once after the formation of massive stars inside the cloud, the I-fronts from the O/B type stars could have expanded into the ambient medium.**
- **Since the magnetic fields were already acquired hour-glass shape, simply the expanding bubble followed the field-lines.**

Summary: NGC 1893

- Optical and NIR polarimetry along with previous results used to understand the dust grain size map the magnetic field orientation in and around NGC 1893

- Magnetic field orientation: I-band and JH-bands suggest: optical polarimetry could be dominated by the foreground dust layers, and the changes in the magnetic field orientation in JH-bands attributed to the changes in the dust grain alignment, and hence change in the magnetic field orientation.

- FG corrected polarization measurements suggest relatively bigger dust grains in NGC 1893

- Field lines are perpendicular to the head-tail region of Sim 129, but are tending to align with tail of Sim 130.

- Sim 130 seems to be affected more, by the I-fronts/winds driven by most luminous O-type star HD 242908, than Sim 129. Further confirmed – tiny BRCs pointing towards HD 242908.

Magnetic Fields at Different Scales:

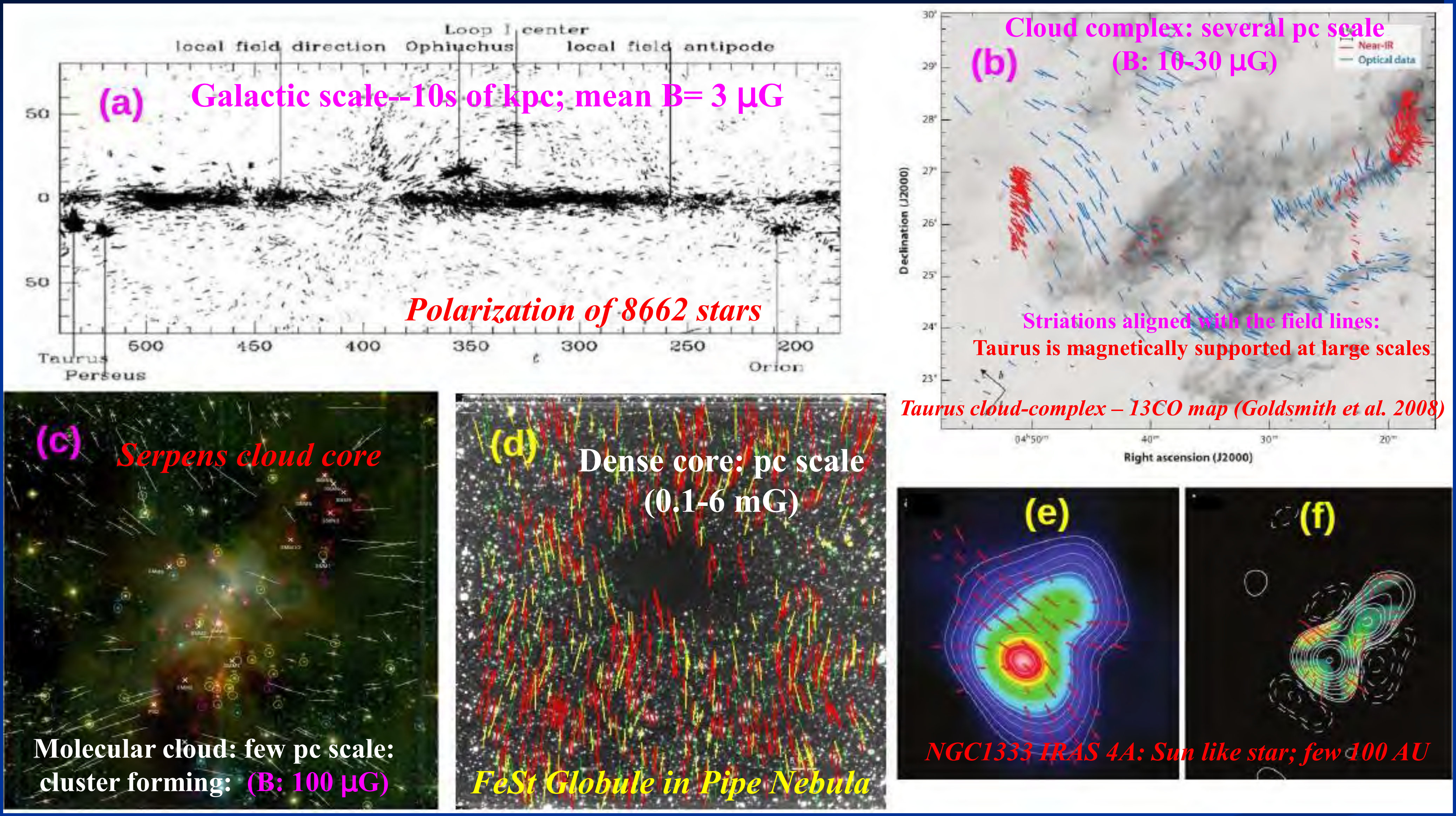

(a) Heiles & Crutcher (2005) (b) Chapman et al. (2011) (c) Sugitani et al. (2010), (d) Clemens et al. (2013, In preparation): NIR H-band polarimetry of FeSt Globule in Pipe Nebula (e) Girart et al. (2006; SMA 0.87 mm) (f) S. P. Lai (Private communication)

Distribution of ISM dust, dust layers, magnetic field

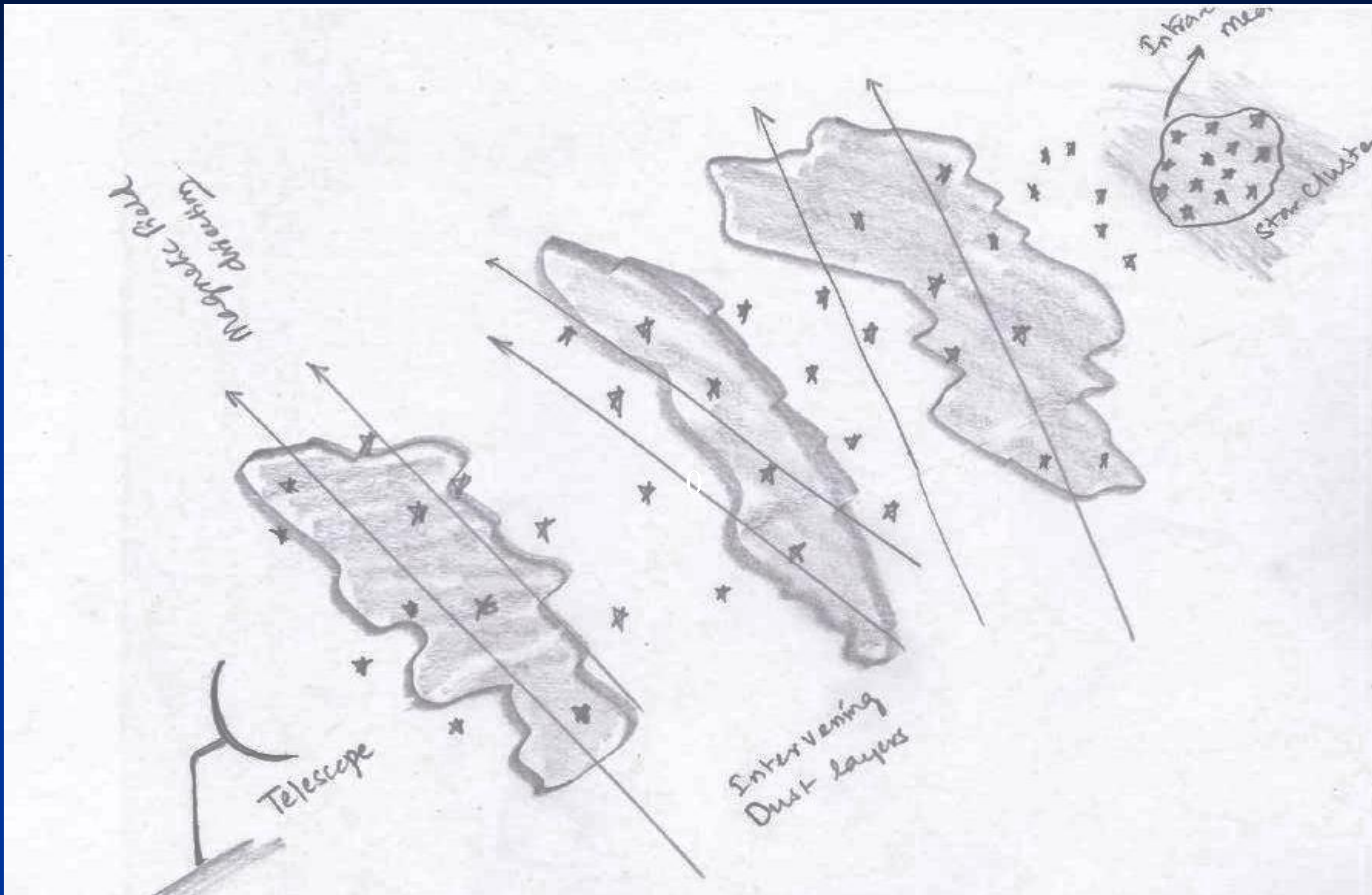

Schematic Diagram: ISM distribution

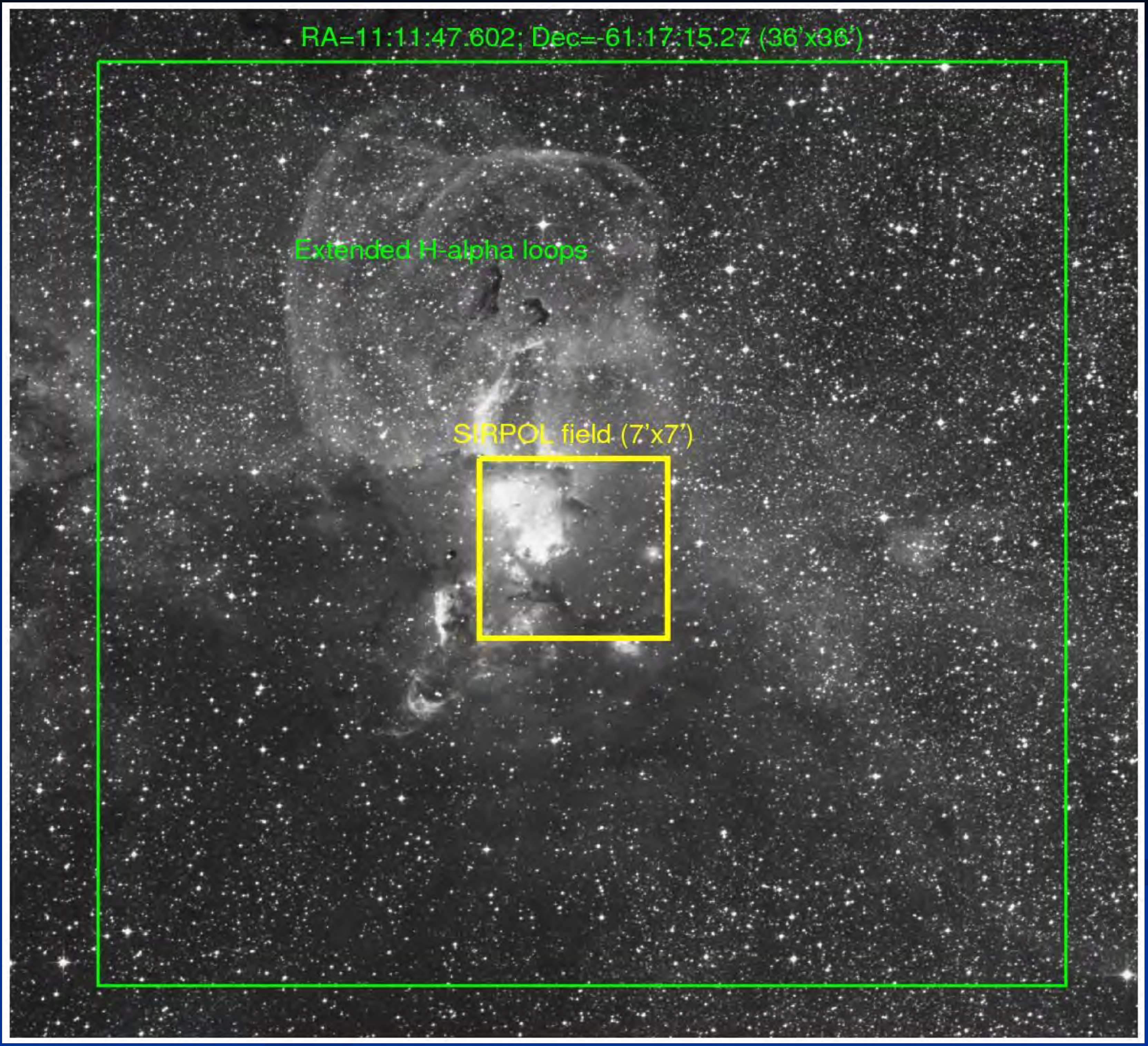
RA=11:11:47.602; Dec=-61:17:15.27 (36'x36')
Extended H-alpha loops
SIRPOL field (7'x7')

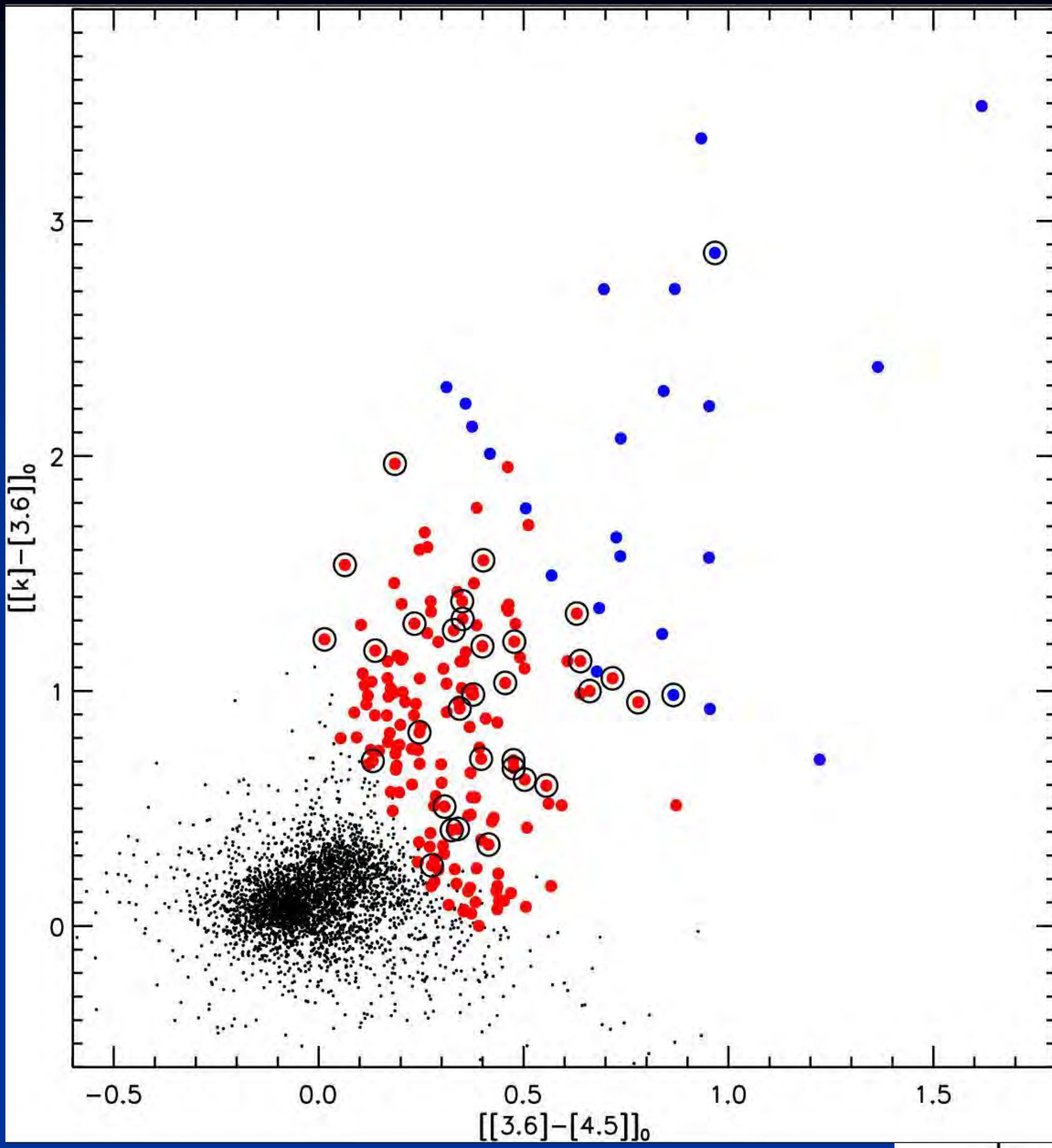

[[k]−[3.6]]0
[[3.6]−[4.5]]0

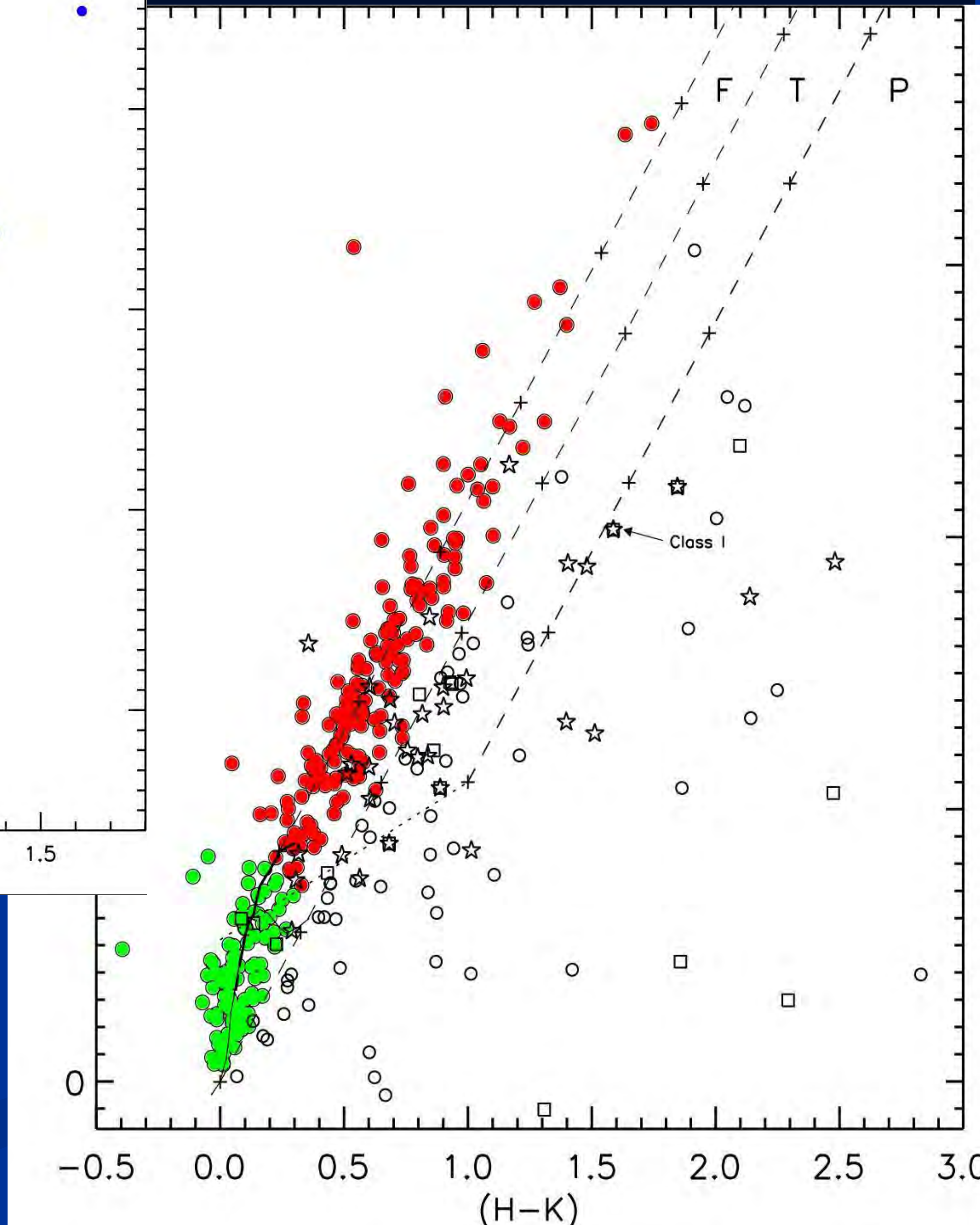

F
T
P
Class I
(H−K)

Observation & Reduction:

To find P (polarization) and θposition angle:

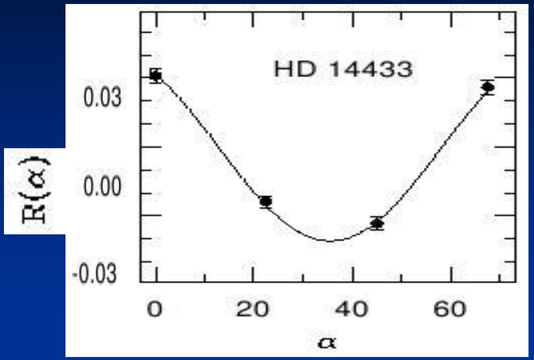

R(α)➔ {*q, u, q1, u1*} at α => 0, 22.5, 45, 67.5 degree

$$R(\alpha) = \frac{I_e/I_o - 1}{I_e/I_o + 1} = p\cos(2\theta - 4\alpha)$$

P% = 4.08 +/- 0.12, θ=109.4 +/- 0.8 degree

σ R(α) {σ q , σ u , σq1 and σu1}

σR(α) = [(Ne + No + 2Nb)/(Ne + No)]^(1/2), (Ramaprakash et al. 1998)

FLAT FIELDING:

$$\frac{I_e(\alpha)}{I_o(\alpha)} = \frac{F_o}{F_e} \times \frac{I_e'(\alpha)}{I_o'(\alpha)}$$

$$\frac{F_o}{F_e} = \left[\frac{I_o'(0^0)}{I_e'(45^0)} \times \frac{I_o'(45^0)}{I_e'(0^0)} \times \frac{I_o'(22.5^0)}{I_e'(67.5^0)} \times \frac{I_o'(67.5^0)}{I_e'(22.5^0)}\right]^{1/4}$$

$I_e'(\alpha)$ and $I_o'(\alpha)$ are actual measured flux.

(Ramaprakash et al. 1998 & Medhi et al 2007, 2010)

Observation & Data Reduction: SIRPOL

J, H, Ks simultaneous, FOV: 7.7x7.7 arcmin^2 observations, three 1kx1k HgCdTe detectors.

Plate scale: 0.45 arcsec/pixel. SIRPOL pipeline – using IRAF and C language

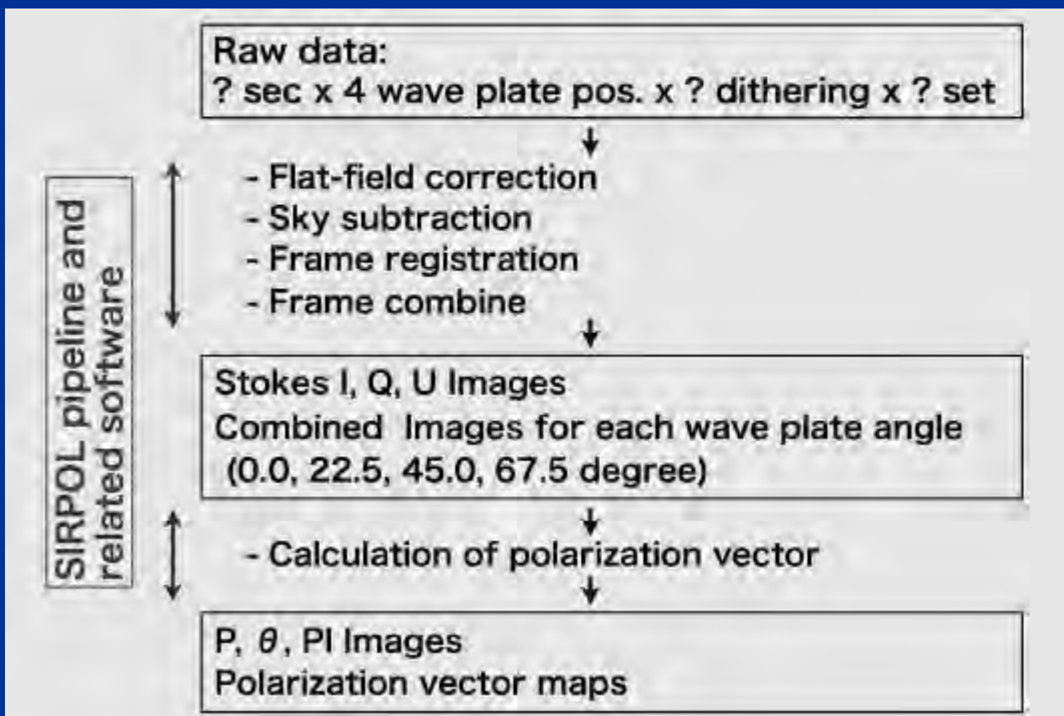

JHKs-bands, 1.25, 1.63, 2.14 micron

Observed on: May 06, 2007

Typical seeing: 1.54, 1.44, 1.35 arcsec
(3.4, 3.2, 3.0 pixels in JHKs bands)

$$
\begin{aligned}
I &= (I_{0.0^\circ} + I_{45.0^\circ} + I_{22.5^\circ} + I_{67.5^\circ})/2 \\
Q &= I_{0.0^\circ} - I_{45.0^\circ} \\
U &= I_{22.5^\circ} - I_{67.5^\circ}
\end{aligned}
$$

$$
\begin{aligned}
P &= \sqrt{Q^2 + U^2}/I \\
\theta &= 0.5 \times \mathrm{atan}(U/Q)
\end{aligned}
$$

(Kandori et al. 2006)

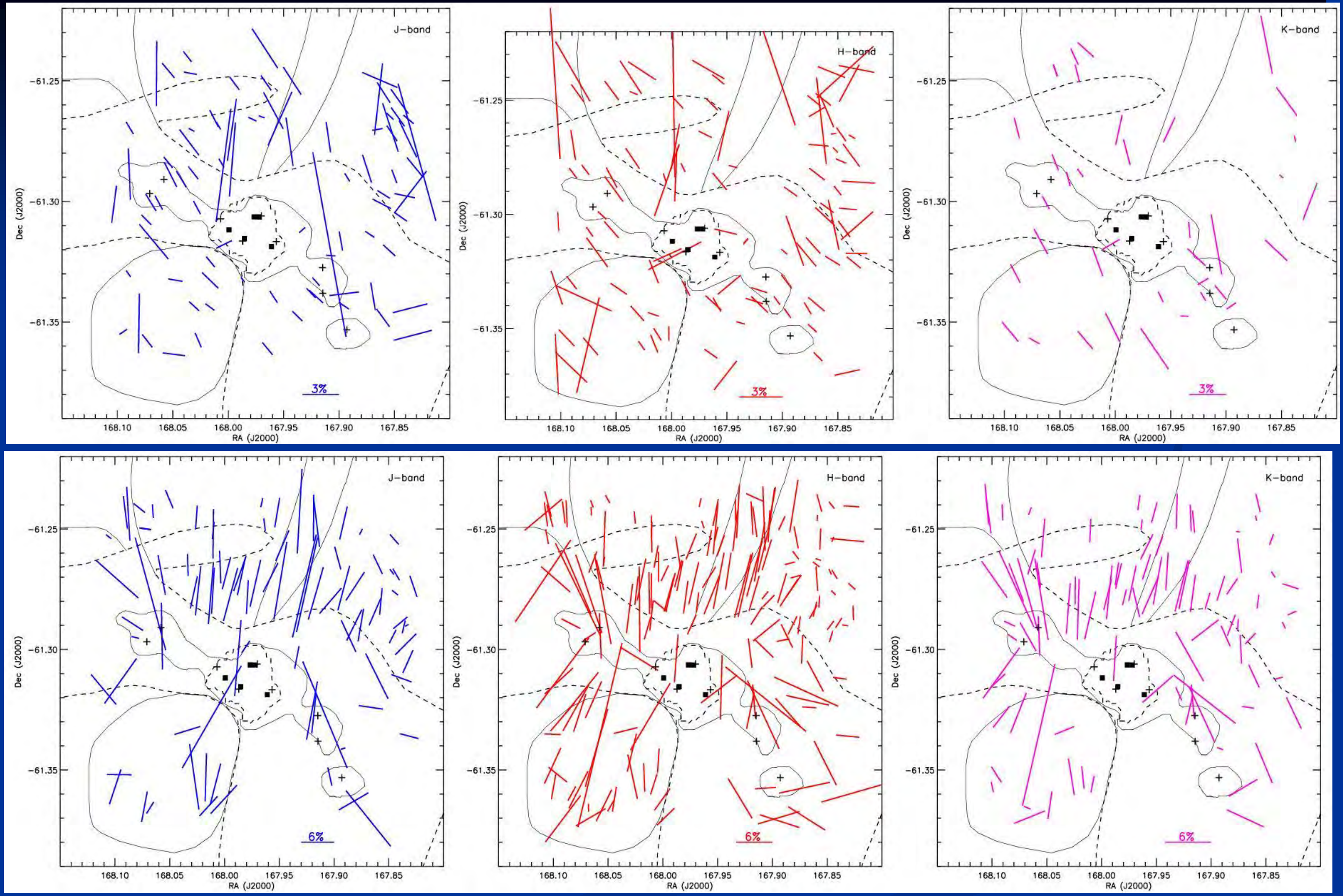

Polarization vector maps of JHKs-bands.

Upper panels: foreground stars; lower panels: background stars

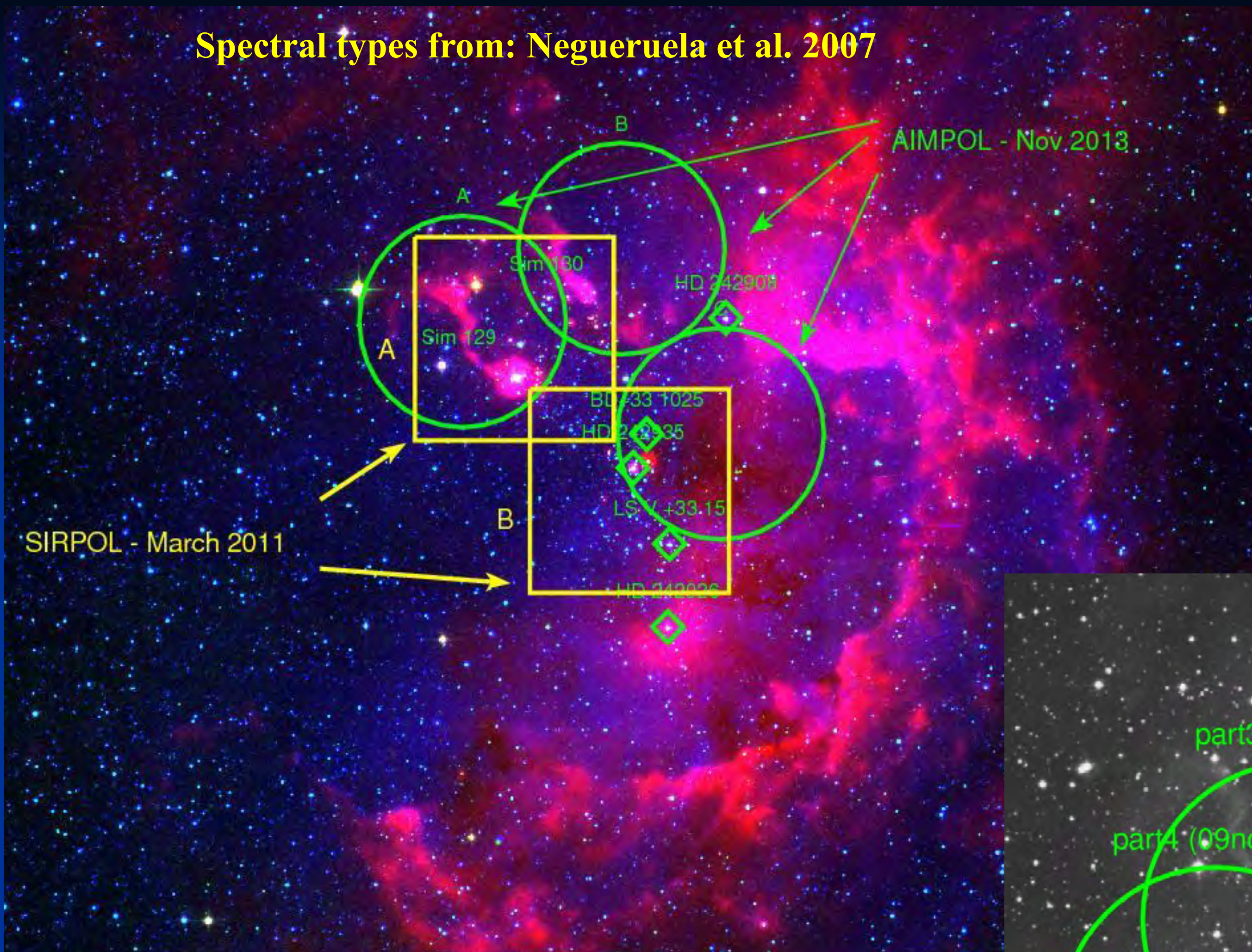
Spectral types from: Negueruela et al. 2007
AIMPOL - Nov 2013
A
B
Sim 130
Sim 129
HD 242908
BD +33 1025
HD 242935
LS V +33 15
HD 242926
SIRPOL - March 2011
A
B

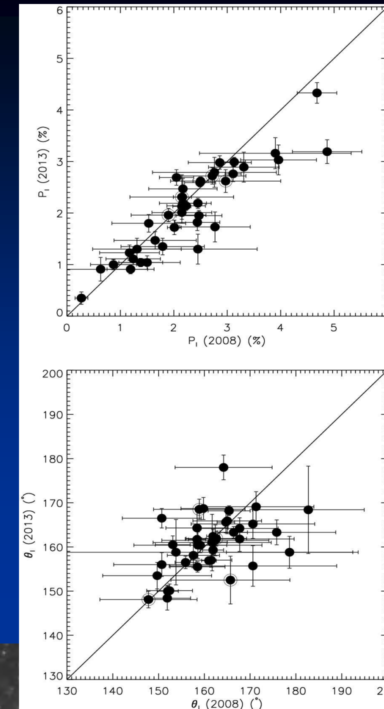
P_i (2013) (%)
P_i (2008) (%)
θ_i (2013) (°)
θ_i (2008) (°)

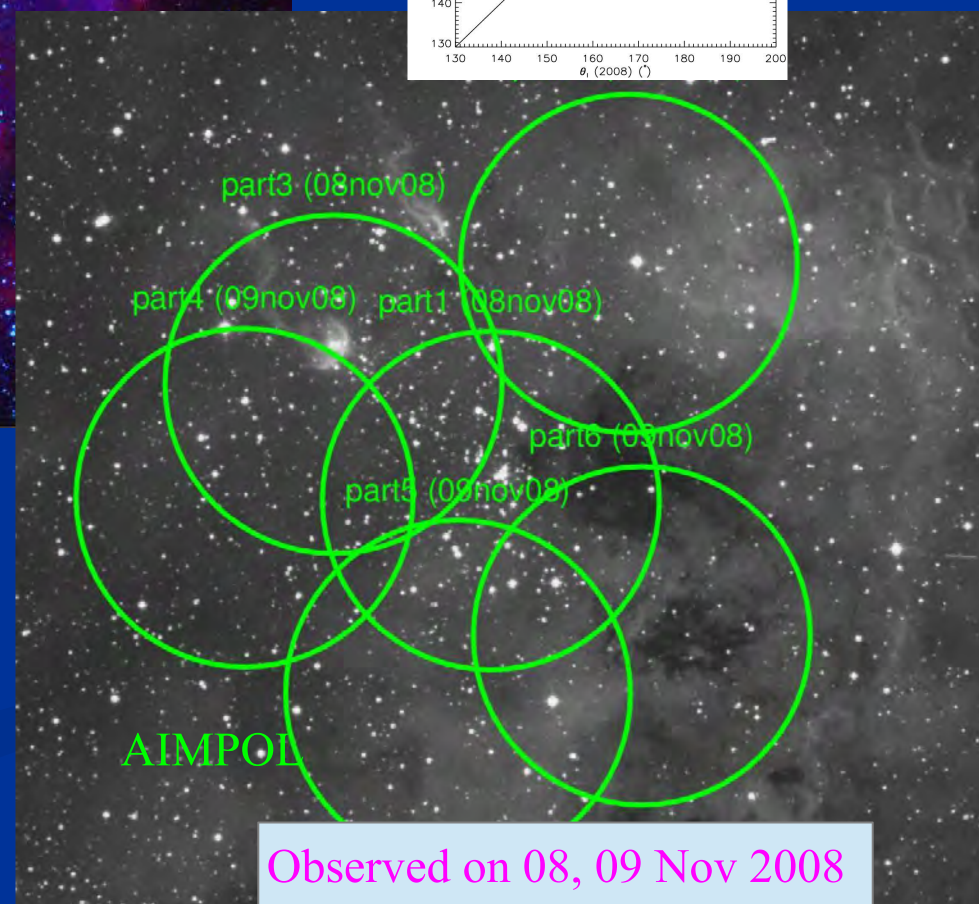
part3 (08nov08)
part4 (09nov08)
part1 (08nov08)
part6 (09nov08)
part5 (09nov08)
AIMPOL
Observed on 08, 09 Nov 2008

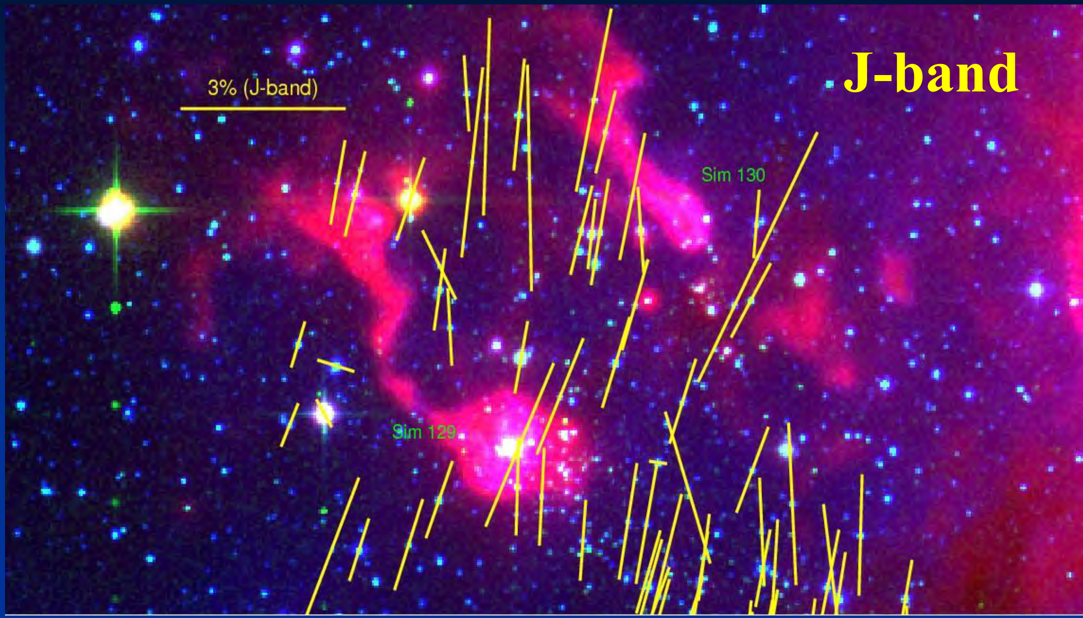

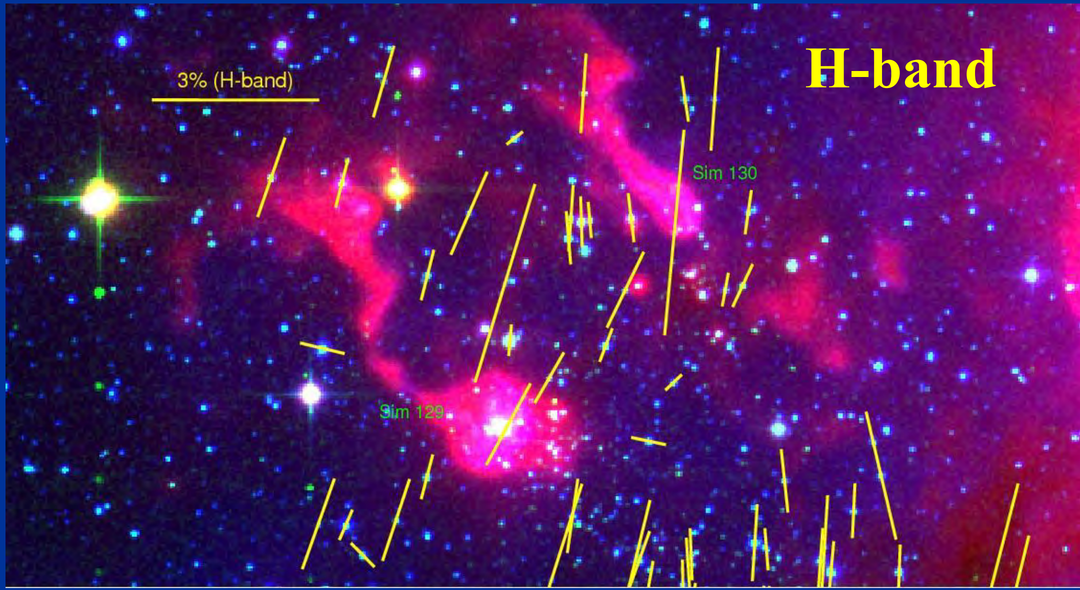

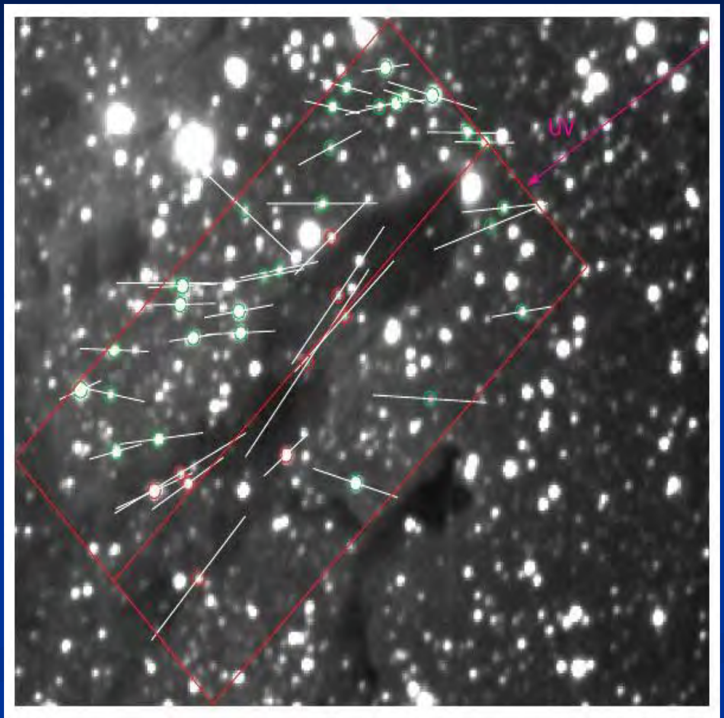

Eagle nebula pillar (Sugitani et al. 2007)

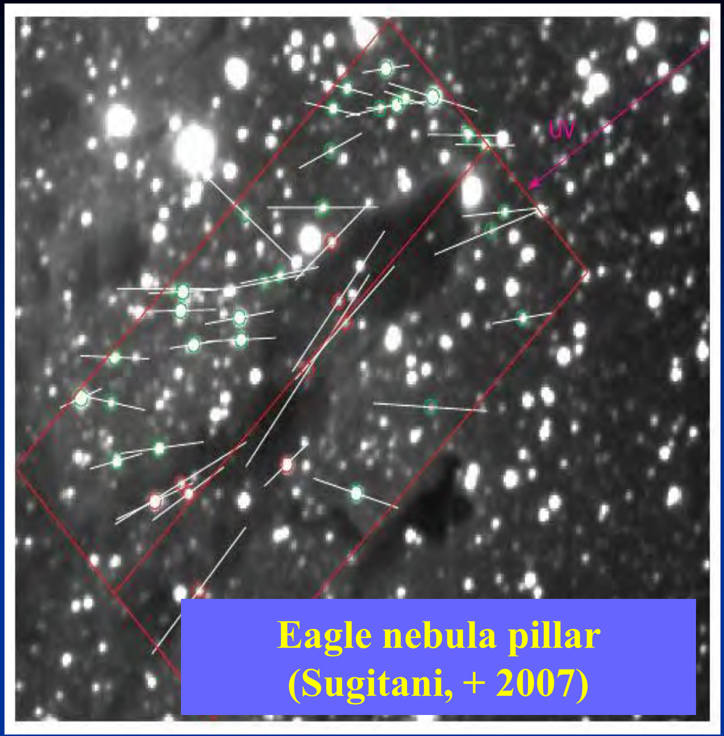

Eagle nebula pillar
(Sugitani, + 2007)

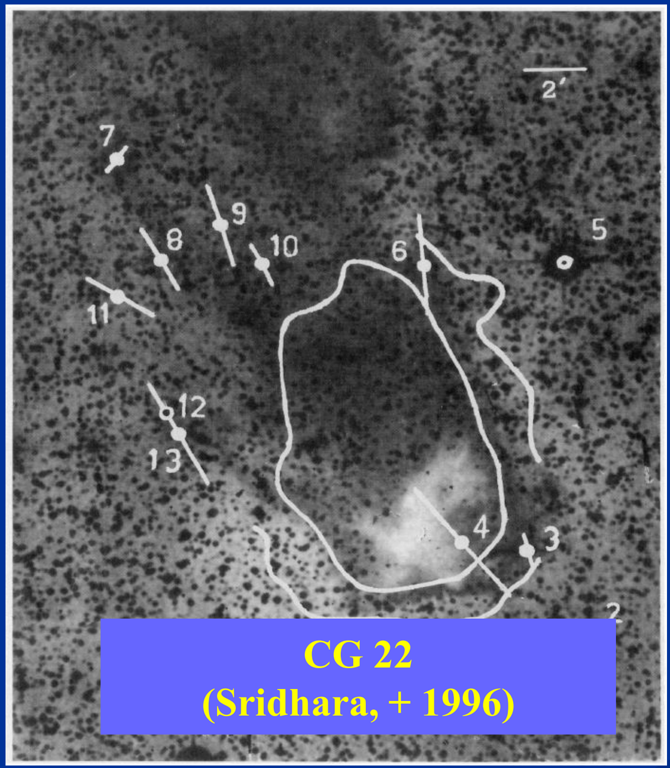

CG 22
(Sridhara, + 1996)

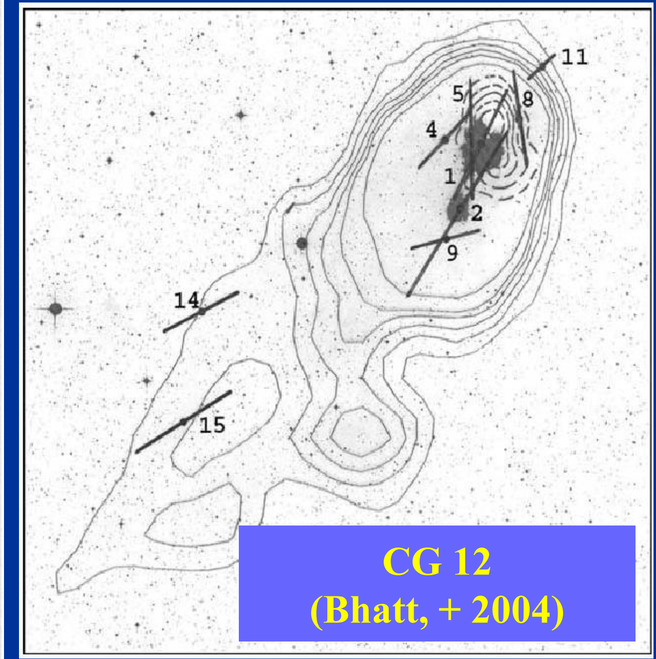

CG 12
(Bhatt, + 2004)

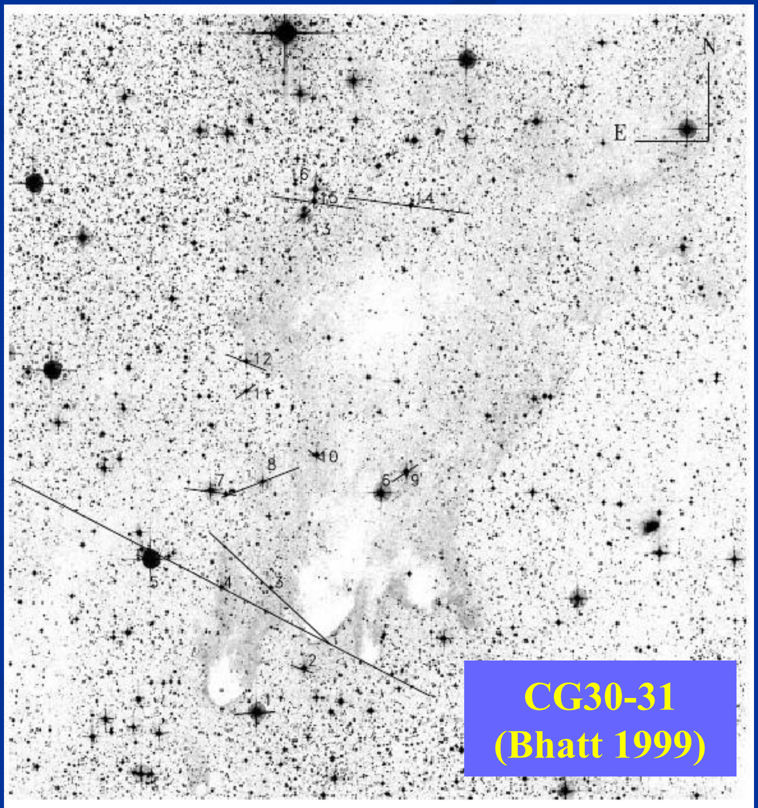

CG30-31
(Bhatt 1999)